Charles University

Faculty of Science

Department of Physical and Macromolecular Chemistry

Doctoral Thesis

MSc. Anastasiia-Bohdana Shatan

Magnetic nanoparticles with antibacterial properties: Synthesis, characterization and biological applications

Supervisor: Ing. Daniel Horák, CSc.

Institute of Macromolecular Chemistry AS CR, v.v.i.

Prague 2024

Univerzita Karlova

Přírodovědecká fakulta

Katedra fyzikální a makromolekulární chemie

Disertační práce

Mgr. Anastasiia-Bohdana Shatan

Magnetické nanočástice s antibakteriálními vlastnostmi: Syntéza, charakterizace a biologické použití

Školitel: Ing. Daniel Horák, CSc.

Ústav makromolekulární chemie AV ČR, v.v.i.

Praha 2024

I hereby declare that this written PhD. thesis is the culmination of my original and independent research conducted under the supervision of Ing. Daniel Horák, CSc. Throughout this endeavor, I have not submitted this work in whole or in part for any other academic degree, diploma or qualification. With the utmost care, I have ensured proper citation of all sources used in this scholarly work to the best of my knowledge.

Prague, March 15, 2024 Anastasiia-Bohdana Shatan

Acknowledgments

I would like to express my sincere gratitude to my esteemed supervisor, Ing. Daniel Horák, CSc., whose guidance and support have been invaluable throughout my PhD. journey. His mentorship has played a pivotal role in shaping my academic endeavors. I am also deeply appreciative of Dr. Vitalii Patsula, PhD., my colleague, whose continuous stream of ideas, positive outlook, and unwavering willingness to assist have been indispensable. This thesis would not have been possible without his invaluable advice, patience, and support.

I extend my heartfelt thanks to the Charles University for providing me with the opportunity to pursue doctoral studies and to the Institute of Macromolecular Chemistry, where I conducted my experimental work. Additionally, I am grateful to all my colleagues, lab-mates, and friends from the Department of Polymer Particles for their insightful discussions and the enjoyable moments we shared over the years.

A special mention goes to my parents, my brother and his family, and my dear grandmother, whose love and encouragement have fueled my pursuit of my dreams. Their unwavering belief in me has been a constant source of strength. Last but certainly not least, I am profoundly thankful to my beloved partner, Orest Kukhar, whose unwavering support has been a beacon during moments of uncertainty. Your presence has been a source of solace and inspiration.

Table of contents

Abstract

In response to the escalating global threat of antibiotic resistance, innovative strategies are imperative. This thesis focuses on surface-engineered magnetic nanoparticles (MNPs) with potent antibacterial properties, aiming to combat antibiotic resistance effectively. Specifically, uniform 16-nm Fe_3O_4 nanoparticles were synthesized via oleic acid-stabilized thermal decomposition of Fe(III) oleate in a high-boiling organic solvent. Optionally, 8-nm γ-Fe_2O_3 particles were obtained by coprecipitation of Fe^{2+} and Fe^{3+} salts in a basic medium. For the application of antibacterial MNPs in biological media, water-dispersible nanoparticles were required. Hence, original magnetic particles containing hydrophobic oleic acid (OA) coating were modified with silica using a water-in-oil reverse microemulsion. Subsequent modification with (3-mercaptopropyl)trimethoxysilane and decoration with silver nanoclusters yielded Fe_3O_4@SiO_2-Ag nanoparticles. Additionally, neat Fe_3O_4 particles were coated with Sipomer PAM-200 containing both phosphate and methacrylic groups, facilitating attachment to the iron oxide and enabling (co)polymerization with 2-(dimethylamino)ethyl methacrylate and/or 2-*tert*-butylaminoethyl methacrylate. Furthermore, γ-Fe_2O_3 nanoparticles were rendered antimicrobial through modification with biocompatible dextran (Dex), to which β-cyclodextrin (β-CD) was covalently linked to form non-covalent complex with silver-sulfamethazine (SMT-Ag). To enhance interaction between β-CD-modified dextran and nanoparticle surface, dextran was functionalized with diphosphonic acid (DPA), ensuring robust binding to Fe atoms.

Comprehensive characterization of the synthesized polymers and nanoparticles was conducted using diverse techniques, including nuclear magnetic resonance (NMR), Fourier-transform infrared (FTIR) and ultraviolet-visible (UV-Vis) spectroscopies, transmission electron microscopy (TEM), thermogravimetric analysis (TGA), atomic absorption spectroscopy (AAS), and dynamic light scattering (DLS). The resulting surface-modified iron oxide nanoparticles were tested *in vitro* demonstrating antimicrobial activity against Gram-positive (*Staphylococcus aureus*) and Gram-negative (*Escherichia coli*) bacteria and fungi (*Candida albicans* and *Aspergillus niger*). The synergistic combination of magnetic properties and bactericidal effects holds promise for applications in medical instrument disinfection, water purification, food packaging, etc.

Keywords: magnetic nanoparticles; polymer; dextran; silver; sulfamethazine; antimicrobial.

Abstrakt

V reakci na eskalující globální hrozbu rezistence bakterií vůči antibiotikům jsou nezbytné inovativní strategie na bázi nonotechnologií. Tato dizertační práce se zaměřuje na povrchově upravené magnetické nanočástice s vysokou antibakteriální aktivitou s cílem účinně bojovat proti rezistenci vůči antibiotikům. Konkrétně byly syntetizovány uniformní 16-nm Fe_3O_4 nanočástice teplotním rozkladem Fe(III) oleátu za stabilizace kyselinou olejovou ve vysokovroucím organickém rozpouštědle. Připraveny byly rovněž 8-nm částice γ-Fe_2O_3 koprecipitací Fe^{2+} a Fe^{3+} solí v zásaditém porostředí. Pro aplikace antibakteriálních částic v biologických médiích bylo zapotřebí, aby byly dobře dispergovatelné ve vodě. Proto byly magnetické částice obsahující hydrofobní povlak kyseliny olejové upraveny silikou v reverzní mikroemulzi voda v oleji. Následovala modifikace (3-merkaptopropyl)trimethoxysilanem a úprava stříbrnými nanoklastry, což vedlo ke vzniku Fe_3O_4@SiO_2-Ag nanočástic. Kromě toho byly holé Fe_3O_4 částice pokryty Sipomerem PAM-200 obsahujícím fosfátové a methakrylátové skupiny usnadňující připojení k oxidu železa a umožňující (ko)polymerizaci s 2-(dimethylamino)ethyl-methakrylátem a/nebo 2-*tert*-butylaminoethyl-methakrylátem. Aby byly γ-Fe_2O_3 nanočástice antimikrobiální, byly modifikovány biokompatibilním dextranem (Dex) s kovalentně navázaným β-cyklodextrinem (β-CD) schopným vytvářet nekovalentní komplexy se sulfamethazinem stříbra (SMT-Ag). Pro zlepšení interakce mezi dextranem s navázaným β-CD a povrchem nanočástic byl dextran modifikován difosfonovou kyselinou, která zajistila pevné ukotvení na Fe atomy částic.

Syntetizované polymery a nanočástice byly důkladně charakterizovány pomocí různých technik, jako je nukleární magnetická rezonance (NMR), infračervená spektroskopie s Fourierovou transformací (FTIR), UV-Vis spektroskopie, transmisní elektronová mikroskopie (TEM), termogravimetrická analýza (TGA), atomová absorpční spektroskopie (AAS) a dynamický rozptyl světla (DLS). Výsledné povrchově modifikované nanočástice oxidu železa byly testovány *in vitro*, kde prokázaly antimikrobiální účinnost proti Gram-pozitivním (*Staphylococcus aureus*) a Gram-negativním (*Escherichia coli*) bakteriím i houbám (*Candida albicans* a *Aspergillus niger*). Synergetická kombinace magnetických a baktericidních vlastností slibuje využití těchto částic pro dezinfekci lékařských nástrojů, čištění vody, potravinářské obaly, atd.

Klíčová slova: magnetické nanočástice; polymer; dextran; stříbro; sulfamethazin; antimikrobiální.

Abbreviations

A. niger	*Aspergillus niger*
AAS	Atomic absorption spectroscopy
ATR-FTIR	Attenuated total reflectance Fourier-transform infrared spectroscopy
C. albicans	*Candida albicans*
CFU	Colony-forming units
Đ	Dispersity
Dex	Dextran
Dex-EA	Ethanolamine-functionalized dextran
Dex-Ts	Tosyl-functionalized dextran
Dex-β-CD	β-Cyclodextrin-functionalized dextran
D_h	Hydrodynamic diameter
DDT	Disk diffusion test
DLS	Dynamic light scattering
DMF	*N,N*-Dimethylformamide
D_n	Number-average diameter
DPA-Dex-β-CD	Diphosphonic acid-modified β-cyclodextrin-functionalized dextran
DVS	Divinyl sulfone
D_w	Weight-average diameter
E. coli	*Escherichia coli*
EA	Ethanolamine
Fe_3O_4@P(DMAEMA-TBAEMA)	Poly[2-(dimethylamino)ethyl methacrylate-*co*-2-*tert*-butylaminoethyl methacrylate]-coated Fe_3O_4
Fe_3O_4@PDMAEMA	Poly[2-(dimethylamino)ethyl methacrylate]-coated Fe_3O_4
Fe_3O_4@SiO_2	Silica-coated Fe_3O_4
Fe_3O_4@SiO_2-Ag	Silver-decorated silica-coated Fe_3O_4
Fe_3O_4@SiO_2-SH	Thiol-functionalized silica-coated Fe_3O_4
Igepal CO-520	Polyoxyethylene(5) nonylphenylether
LA	Luria agar
LB	Luria broth
MBC/MMC	Minimum bactericidal/microbicidal concentrations
MIC	Minimum inhibitory concentration
M_n	Number-average molecular weight

MNPs	Magnetic nanoparticles
MPTMS	(3-Mercaptopropyl)trimethoxysilane
MRI	Magnetic resonance imaging
M_s	Saturation magnetization
M_w	Weight-average molecular weight
NMR	Nuclear magnetic resonance
OA	Oleic acid
OD	Octadec-1-ene
PD	Polydispersity
PDMAEMA	Poly[2-(dimethylamino)ethyl methacrylate]
PTBAEMA	Poly(2-*tert*-butylaminoethyl methacrylate)
RT	Room temperature
S. aureus	*Staphylococcus aureus*
SIPO	Sipomer PAM-200
SMT	Sulfamethazine
SMT-Ag	Silver-sulfamethazine
TEM	Transmission electron microscopy
TGA	Thermogravimetric analysis
THF	Tetrahydrofuran
TMOS	Tetramethyl orthosilicate
Ts	Tosyl
TsCl	Tosyl chloride
Ts_2O	p-Toluenesulfonic anhydride
XPS	X-ray photoelectron spectroscopy
β-CD	β-Cyclodextrin
β-CD-EA	Ethanolamine-functionalized β-cyclodextrin
β-CD-Ts	Tosyl-functionalized β-cyclodextrin
β-CD-VS	Vinyl sulfone-functionalized β-cyclodextrin
γ-Fe_2O_3@DPA-Dex-β-CD	γ-Fe_2O_3 coated with diphosphonic acid-modified β-cyclodextrin-functionalized dextran
γ-Fe_2O_3@DPA-Dex-β-CD-SMT-Ag	γ-Fe_2O_3 coated with diphosphonic acid-modified β-cyclodextrin-functionalized dextran and silver-sulfamethazine

List of author's publications

1. Shatan A.B., Venclíková K., Zasońska B.A., Patsula V., Pop-Georgievski O., Petrovský E., Horák D., Antibacterial silver-conjugated magnetic nanoparticles: Design, synthesis and bactericidal effect, *Pharm. Res.* 36, 147, **2019** (IF = 3.7). doi:10.1007/s11095-019-2680-x

2. Shatan A.B., Patsula V., Dydowiczová A., Gunár K., Velychkivska N., Hromádková J., Petrovský E., Horák D., Cationic polymer-coated magnetic nanoparticles with antibacterial properties: Synthesis and *in vitro* characterization, *Antibiotics* 10, 1077, **2021** (IF = 4.8). doi:10.3390/antibiotics10091077

3. Shatan A.B., Patsula V., Macková H., Mahun A., Lehotská R., Piecková E., Horák D., Silver-sulfamethazine-conjugated β-cyclodextrin/dextran-coated magnetic nanoparticles for pathogen inhibition, *Nanomaterials* 14, 371, **2024** (IF = 5.3). doi:10.3390/nano14040371

Other author's publications

1. Velychkivska N., Sedláček O., Shatan A.B., Spasovová M., Filippov S.K., Chahal M.K., Janisova L., Brus J., Hanyková L., Hill J.P., Winnik F.M., Labuta J., Phase separation and pH-dependent behavior of four arm star shaped porphyrin PNIPAM4 conjugates, *Macromolecules* 55, 2109-2122, **2022** (IF = 6.057). doi:10.1021/acs.macromol.1c02188

2. Komatsu H., Velychkivska N., Shatan A.B., Shindo Y., Oka K., Ariga K., Hill J.P., Labuta J., Kinetic study of NADPH activation using ubiquinone-rhodol fluorescent probe and an IrIII-complex promoter at the cell interior, *RSC Adv.* 13, 34012-34019, **2023** (IF = 4.036). doi:10.1039/D3RA05412H

Oral presentations at conferences

1. Shatan A.B., Zasońska B.A., Horák D., Antibacterial magnetic nanoparticles: Design, synthesis and bactericidal effect, Career in Polymers X, Prague, Czech Republic 2018, Abstract Book, L-11.

2. Shatan A.B., Zasońska B.A., Horák D., Magnetic nanoparticles with antibacterial properties: Design, synthesis and bactericidal effect, Conference of Young Scientists at EastWest Chemistry Conference, Lviv, Ukraine 2018, Abstract Book, p. 42.

3. Horák D., Ma Y.H., Świętek M., Shatan A.B., Moskvin M., Antioxidant and antibacterial magnetic nanoparticles: Design, synthesis and biological effects, International Conference on

the Scientific and Clinical Applications of Magnetic Carriers, London, United Kingdom, 2022, Abstract Booklet, Talk 60.

Poster presentations

1. Shatan A.B., Horák D., Design, synthesis and bactericidal activity of polymer-coated magnetic nanoparticles, Frontiers of Polymer Colloids: From Synthesis to Macro-Scale and Nano-Scale Applications, 84th Prague Meeting on Macromolecules, Prague, Czech Republic 2022, Abstract Book, p. 129.

2. Shatan A.B., Horák D., Bactericidal activity of polymethacrylate-coated magnetic nanoparticles, 5th RECOOP International Student and 18th RECOOP Bridges in Life Sciences Conferences, Budapest, Hungary 2023, Abstract Book, p. 49.

1. Introduction

Since the 1940s, when antibiotics were first used to treat serious infections and transformed modern medicine, they have saved millions of lives and made many infectious diseases far less deadly. Recently, physician offices and emergency departments only in the United States prescribe about 47 million antibiotics each year for infections that do not need antibiotics, according to the Centers for Disease Control and Prevention[1]. As a result, bacteria have developed resistance to antibiotics, which is now a major threat for public health as traditional drugs are becoming less and less effective[2,3]. Antibiotic-resistant bacteria can reach humans through various routes of transmission, such as air, soil and, most commonly, water. It is therefore worth mentioning that in remote areas of the world, disinfection of drinking water using new techniques that destroy pathogens is becoming increasingly important. For this purpose, particles with sterilizing properties are used based on silver, copper, various metal oxides or sulfides or carbon nanotubes[4]. Other physical methods for purifying contaminated water include filtration, thermal treatment and UV irradiation. However, these approaches have disadvantages such as time-consuming, high cost, waste of resources and the need for various additives and reagents[5]. In a search for novel, potent and simple solutions of these problems, a significant effort has been devoted to the development of new antibacterial agents based on various nanoparticles, which can mimic biological protein inhibitors by matching their sizes, geometries and surface chemistry[6]. In contrast to traditional antibiotics, these new agents exhibit exclusive physicochemical and biological properties. These include remarkable chemical and colloidal stability as well as the possibility to bind target compounds, ligands and various biomolecules via different functional groups. In addition, the increased surface-to-volume ratio enhances the interaction with microorganisms, allowing, for example, the disinfection of various devices. Among the variety of developed nanoparticles with antibacterial properties, the magnetic ones are of particular interest due to their unique advantage of being able to be monitored by magnetic resonance imaging (MRI) and targeted to the desired sites by an external magnetic field[7].

1.1. Magnetic nanoparticles (MNPs)

From a wide variety of existing nanoparticle types, the magnetic ones show great potential for different biomedical applications, such as biomolecule separation, targeted drug delivery, tissue repair, cell labeling, hyperthermia, treatment of cardiovascular diseases and MRI[8]. The unique characteristics of MNPs include small size, large surface area, low toxicity,

and responsiveness to external magnetic fields. There is also great interest to explore applicability of MNPs as carriers of antibacterial polymers and antibiotics to fight multidrug-resistant bacteria. By using an external magnetic field to guide the MNPs to the targeted bacteria, infections that are resistant to traditional antibiotics can be treated more efficiently and with fewer side effects[9,10]. In addition, MNPs can deliver multiple drugs at once, increasing the effectiveness of the treatment and reducing the risk of the bacteria developing a resistance[11]. The MNPs typically consist of ferromagnetic elements like iron, cobalt, and nickel, the latter two elements not being ideal for biomedical applications due to possible toxicity. In particular, non-toxic surface-engineered superparamagnetic iron oxide nanoparticles, such as magnetite (Fe_3O_4) or maghemite (γ-Fe_2O_3), have shown considerable potential, as they allow high drug doses to be delivered, increasing the chances of successful treatment while reducing side effects. There are many types of iron oxides, but only three of them are very promising for various biomedical applications. These include:

Hematite (α-Fe_2O_3) is a prevalent and highly stable form of iron oxide, characterized by a rhombohedral lattice structure (Figure 1). Under normal conditions, α-Fe_2O_3 exhibits n-type semiconductor behavior with a band gap of 2.3 eV[12]. The valence band of hematite consists of a mixture of occupied 3d orbitals from Fe^{3+} and 2p nonbonding orbitals from O^{2-}, while the conduction band contains only empty d-orbitals of Fe^{3+}. Apart from its semiconductor properties, α-Fe_2O_3 finds wide-ranging applications such as biomedical, photocatalysis and environmental sensing[13]. Furthermore, hematite plays a crucial role in the synthesis of other important iron oxide materials like magnetite and maghemite.

Magnetite (Fe_3O_4) has a face-centered cubic spinel structure with a closely packed arrangement of 32 O^{2-} ions along specific directions (Figure 1). Magnetite coexist with both divalent (Fe^{2+}) and trivalent (Fe^{3+}) forms of iron within its crystal structure. Specifically, half of the octahedral sites are occupied by divalent iron ions, while the trivalent iron ions are evenly distributed across the remaining octahedral and tetrahedral sites. Magnetite exhibits versatile semiconductor behavior, acting as both an n-type and p-type semiconductor. This is owing to its stoichiometric alloy nature, where the molar ratio of Fe^{2+} to Fe^{3+} is 1:2. Consequently, the divalent iron ions can be substituted with other divalent ions like Zn, Co, and Ni. Moreover, magnetite possesses an exceptionally small band gap of only 0.1 eV, resulting in the lowest resistivity among all iron oxide forms[14].

Maghemite (γ-Fe_2O_3) has a cubic structure; its each unit contains 32 O^{2-} ions, 21⅓ Fe^{3+} ions and 2⅓ vacancies. Oxygen anions give rise to a cubic close-packed array while ferric ions are distributed over tetrahedral sites (eight Fe ions per unit cell) and octahedral sites (the

remaining Fe ions and vacancies)[15]. Therefore, the maghemite can be considered as fully oxidized magnetite, and it is an n-type semiconductor with a band gap of 2.0 eV.

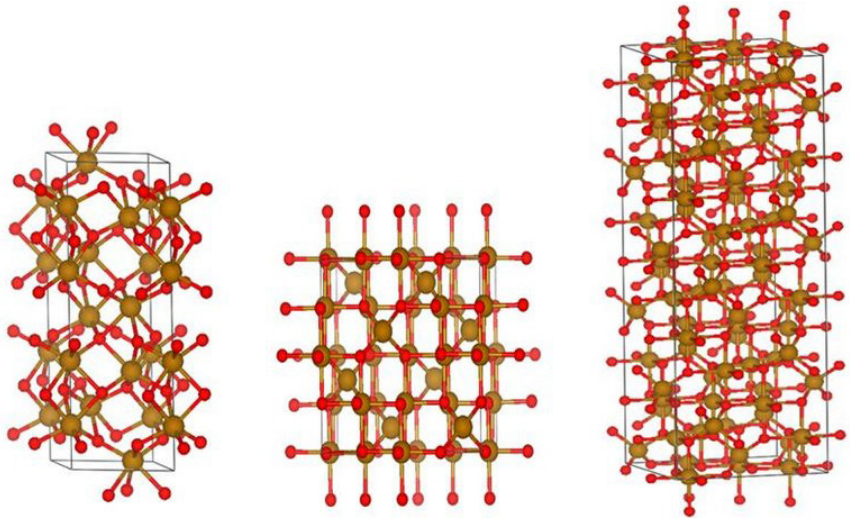

Figure 1. Atomic structure of different MNPs. Taken from[16].

1.2. Properties of MNPs

Magnetic properties include the behavior and characteristics of materials in response to magnetic fields. These characteristics stem from the presence of magnetic moments inherent in certain materials at either the atomic or molecular level. Other key magnetic property of particles includes magnetization. A magnetic field is a region around a magnetic object or a current-carrying conductor where the magnetic force is exerted. The magnetic field is typically represented by magnetic field lines that indicate the direction of the force experienced by a magnetic object in that region. A magnetic moment is a measure of the strength and orientation of the magnetic field generated by an atom, molecule, or particle. It is a vector quantity and indicates the direction of the magnetic field produced by the material[16].

Magnetic materials can be classified into three main categories based on their response to an external magnetic field (Figure 2). (*i*) Diamagnetic materials have weak negative magnetic susceptibility, which means they tend to generate a weak magnetic field in the opposite direction to an applied magnetic field. (*ii*) Paramagnetic materials have weak positive magnetic susceptibility, leading to a weak magnetic field in the same direction as an applied magnetic field. (*iii*) Ferromagnetic and ferrimagnetic materials have strong positive magnetic susceptibility and exhibit spontaneous magnetization even in the absence of an external magnetic field[16]. Ferromagnetic and ferrimagnetic materials possess permanent magnetic

moments that are aligned in a specific pattern, leading to spontaneous magnetization. In ferromagnetic materials, adjacent magnetic moments align parallel, whereas in ferrimagnetic materials, adjacent magnetic moments align anti-parallel, resulting in net magnetization. The Curie temperature is the critical temperature at which a ferromagnetic or ferrimagnetic material undergoes a phase transition from a magnetically ordered state to a paramagnetic state. Above this temperature, the material loses its spontaneous magnetization. Magnetic hysteresis is then the phenomenon observed in ferromagnetic materials, where magnetization lags behind changes in the applied magnetic field. This lagging effect causes the material to retain some magnetization even after the external field is removed[17].

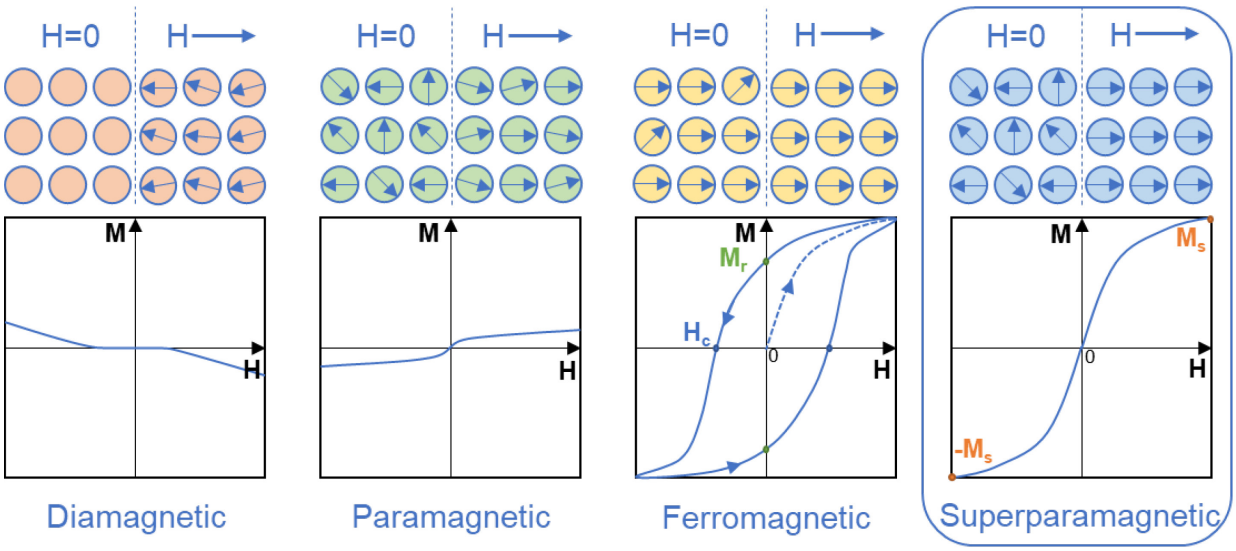

Figure 2. Examples of the behavior of different materials in magnetic fields[18].

Superparamagnetic materials are specific in that they exhibit unique magnetic behavior due to their small size and the effect of thermal fluctuations. Unlike traditional magnetic materials that retain their magnetization even after the removal of an external magnetic field, superparamagnetic particles do not have a permanent magnetic moment in the absence of an external field[19]. Instead, they display dynamic behavior depending on temperature and magnetic fields. Key features of superparamagnetic materials include (*i*) size dependence. Superparamagnetism is most pronounced in nanoscale materials, typically in the range of a few nanometers to a few tens of nanometers. As the particle size decreases, the effect of thermal energy becomes more significant, causing the magnetic moments of individual particles to fluctuate more rapidly[20]. (*ii*) Lack of remanence and coercivity. Remanence refers to the residual magnetization retained by a material after removal of the external magnetic field, and coercivity is a measure of the material resistance to demagnetization. Superparamagnetic

materials have very low or negligible remanence and coercivity. (*iii*) No hysteresis. Unlike ferromagnetic materials that exhibit hysteresis and retain magnetization after an external field is applied and removed, superparamagnetic materials do not exhibit hysteresis loops. This is because their magnetization can rapidly switch direction in response to temperature changes. (*iv*) Thermal fluctuations. At the nanoscale, thermal energy in the surrounding environment can overcome the energy barrier that would otherwise stabilize the alignment of magnetic moments. This means that the magnetic moments of particles can change direction randomly due to thermal fluctuations, even in the absence of an external magnetic field[16,19]. It is worth to mention that iron oxide nanoparticles (γ-Fe_2O_3 and Fe_3O_4) demonstrate superparamagnetic behavior at a size <20 nm[21]. Furthermore, such nanoparticles do not exhibit magnetically induced aggregation when dispersed in aqueous media. Hence, this makes superparamagnetic nanomaterials an ideal tool for various biomedical applications.

1.3. Synthesis of iron oxide nanoparticles

The choice of synthesis method is important as it significantly affects the properties of MNPs. Different techniques offer varying degrees of control over factors such as particle size, particle size distribution, morphology and crystalline structure. A lot of different methods have already been described for the synthesis of iron oxides, such as coprecipitation, thermal decomposition, microemulsion, sol-gel, hydrothermal synthesis, electrochemical synthesis and biological synthesis (green approach), each with its own advantages and disadvantages[15,22]. However, the most commonly used methods are coprecipitation of iron salts and the thermal decomposition of organic iron precursors.

A key technique for the preparation of magnetic iron oxide nanoparticles is the coprecipitation of Fe^{2+} and Fe^{3+} salts with a base such as NaOH or NH_4OH (Scheme 1). Although primarily magnetite (Fe_3O_4), which is unstable in air and water, is formed, its controlled oxidation with, for example, sodium hypochlorite is preferred to form maghemite (γ-Fe_2O_3). A critical aspect in the formation of a stable magnetite/maghemite colloid is careful purification and washing with water to remove residual impurities after synthesis; this process, which uses magnetic separation, is referred to as “peptization”. The coprecipitation method allows the preparation of particles in the size range of 5-20 nm depending on factors such as the type of iron salt (chloride, sulfate, nitrate), the molar ratio of Fe^{2+}/Fe^{3+}, pH, ionic strength, and temperature[23]. Alternatively, in the case of acidic colloid preparation, Fe_3O_4 precipitate is mixed with aqueous perchloric acid. The advantage of the coprecipitation method lies in obtaining large amounts of hydrophilic particles with good magnetic properties and in the use

of cost-effective starting materials. However, the limitation is in the wide particle size distribution, which leads to irregular magnetic behavior.

$$Fe^{2+} + 2\,Fe^{3+} + 8\,OH^- \rightarrow Fe_3O_4 + 4\,H_2O$$

$$2\,Fe_3O_4 + {}^1/_2\,O_2 \rightarrow 3\,\gamma\text{–}Fe_2O_3$$

Scheme 1. Synthesis of γ-Fe_2O_3 nanoparticles by coprecipitation and oxidation.

Another important technique for the preparation of iron oxide nanoparticles is the high-temperature decomposition of organic iron precursors such as Fe(III) oleate. Other precursors may include Fe(III) carboxylates, $Fe(CO)_5$, Fe(III) *N*-nitroso-*N*-phenylhydroxylamine or Fe(III) acetylacetonate[24]. These syntheses are performed in a high-boiling solvent, typically octyl ether or octadec-1-ene, in the presence of a stabilizing agent, such as oleic acid or oleylamine[25] (Figure 3). The method enables the production of uniform MNPs with high crystallinity and allows precise control of their size, commonly ranging from 2 to 30 nm. The properties of these MNPs depend on various factors, including the reaction temperature and time, the type of solvent, the specific iron precursor, and the stabilizing agent, as well as their initial proportions in the reaction mixture[24]. The mechanism of the synthesis involves three main stages. (*i*) Initially, the thermal decomposition of an iron precursor occurs at elevated temperatures, which leads to the formation of poly(iron oxo) clusters, serving as the fundamental building blocks for the nanoparticles. (*ii*) Afterward, there is a rapid and intense nucleation period known as “short burst nucleation”. (*iii*) Finally, as the temperature is further increased, the nanoparticles grow by incorporating additional nuclei[26]. The resulting MNPs exhibit a monodisperse distribution in size due to the combination of a short nucleation period and the presence of the stabilizing agent. The stabilizer prevents the aggregation of nuclei and ensures uniform growth conditions for each particle. However, it should be noted that a disadvantage of the thermal decomposition method is the requirement for high synthesis temperature and the presence of a hydrophobic coating on the nanoparticles, which requires its replacement with a hydrophilic one to make the particles dispersible in water.

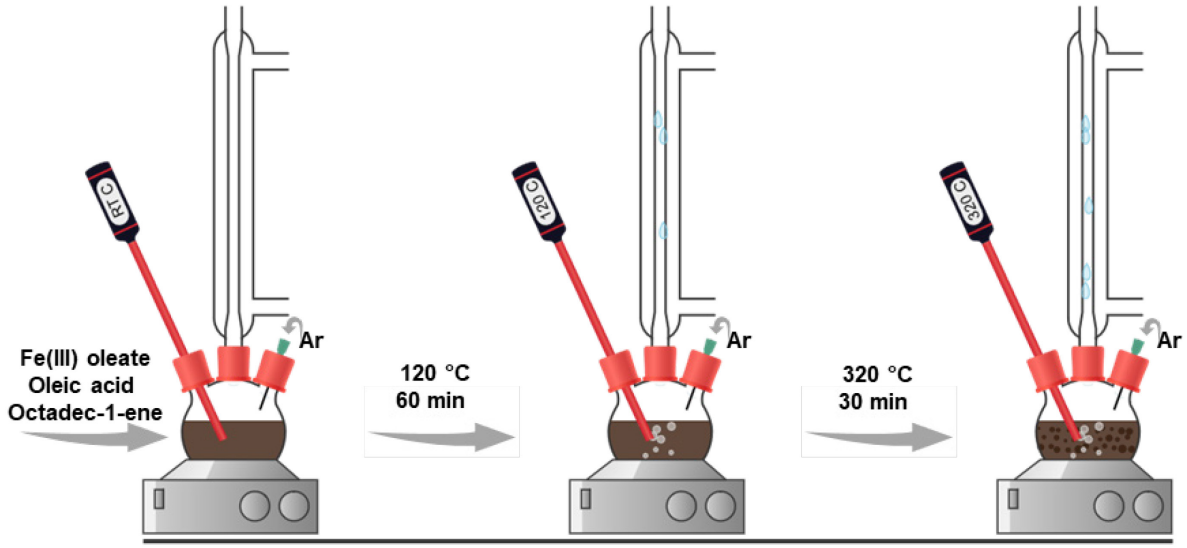

Figure 3. High-temperature thermal decomposition of Fe(III) oleate.

Many alternative techniques for the synthesis of MNPs include, but are not limited to, solvo(hydro)thermal method, sol-gel reactions, microwave approach and biosynthesis. In the solvo(hydro)thermal process, e.g. based on the reduction of $FeCl_3$ with ethylene glycol, controllable particle sizes are available on the submicrometer scale (200-800 nm)[27]. The disadvantages are synthetic conditions in an autoclave usually requiring long reaction times (<10 h) and high temperatures (up to 200 °C). Therefore, a microwave-assisted method was developed to dramatically accelerate the growth of magnetic particles, which is completed within minutes. In the water-in-oil microemulsion technique, an aqueous phase containing iron precursors is dispersed in a continuous organic phase in the form of microdroplets (1-50 nm in size) surrounded by a stabilizer. By adding a solvent to the microemulsion, the precipitate can be separated by filtration or centrifugation[28]. Electrochemical synthesis of MNPs involves the controlled deposition of iron ions onto electrodes immersed in an electrolyte solution[29]. Typically, an anode undergoes oxidation to release metal ions into the solution, which are then reduced to form iron oxide nanoparticles at the cathode. The process offers precise control over particle size and high purity of the resulting nanoparticles. While it operates at relatively low temperatures and provides excellent control over the synthesis process, it may not be suitable for large-scale production due to certain limitations, and the synthesized nanoparticles may contain some amorphous components[30]. Recently, biosynthesis of biocompatible MNPs using magnetotactic bacteria, e.g., *Pseudomonas aeruginosa*, isolated from lakes, soil, seas, and sunken mud, represents a cheap and environmentally friendly approach[31].

Since antibacterial magnetic nanoparticles for biomedical applications must meet specific criteria such as biocompatibility and small particle size, coprecipitation and thermal decomposition methods were chosen in this work. These techniques allow the generation of small (<20 nm) iron oxide nanoparticles on a large scale and the use of affordable non-toxic iron precursors, i.e. Fe(III) and Fe(II) chlorides and Fe(III) oleate. The particle size ranging from 10-30 nm is also important in terms of avoiding rapid renal clearance or magnetic aggregation of particles >30 nm.

1.4. Surface modification of MNPs

The functioning of MNPs is dependent on many factors, such as shape, size, large surface-to-volume ratio, and the presence of reactive functional groups allowing the binding of various target biological substances in sufficient quantities. At the same time, it is necessary to maintain colloidal stability of MNPs in biologically relevant aqueous media for extended periods of time, which can be challenging as the particles tend to aggregate or precipitate. In addition, it is important to minimize non-specific adsorption of proteins and cells. There are basically two types of stabilization, electrostatic and steric (Figure 4). The first type is achieved by electrostatic charges on the surface of the nanoparticles, e.g., from chlorate, citrate, and nitrate anions or tetramethylammonium cations; the product is then called as an acidic or basic ferrofluid[32]. However, the stability thus achieved is very sensitive to the presence of other electrolytes in the supernatant, so it is necessary to keep the pH within a narrow range and use a solution with low ionic strength. Therefore, colloidal stability and compatibility of particles with living tissues are usually achieved by a protective coating, grafting or encapsulation of MNPs. Coating of organic materials on the MNP surface is done *in situ* (typically by miniemulsion polymerization or sol–gel process) or after synthesis, which is more common[32]. The latter approach is exemplified by the physical adsorption of low- or high-molecular weight compounds or employing functional groups for covalent binding of amphiphilic copolymers. The protective coating not only prevents oxidation and degradation of particles, but also allows further modifications with drugs, biomolecules (enzymes, proteins, polypeptides, antibodies, biotin, avidin and albumin) or catalytically active components[33]. Several methods have been used to produce surface-modified MNPs, including binding of low-molecular-weight compounds, e.g., *D*-mannose[34] or dimercaptosuccinic acid[35]. Another possibility is the adsorption of biomolecules and/or binding of various polymers such as poly(vinyl alcohol), poly(ethylene glycol), poly(acrylic acid), poly(*D*,*L*-lactide), polyethylenimine, poly(4-styrenesulfonic acid-*co*-maleic acid), poly(*L*-lysin), dextran, starch, chitosan, or silica[32,36,37].

The latter is often used due to its noncytotoxicity, high chemical stability, reasonable price, simple synthesis, and ability to be easily modified with various functional groups. Silica is often coated on the MNPs by Stöber method where SiO_2 is formed by *in situ* hydrolysis and condensation of a sol-gel precursor, such as tetraethoxysilane (TEOS), vinyltriethoxysilane, 3-aminopropyltriethoxysilane, *p*-aminophenyltrimethoxysilane, mercaptopropyltriethoxysilane, or (3-glycidyloxypropyl)trimethoxysilane[15]. In the case of dextran-coated MNPs, the great advantage is that they have been approved by the FDA for clinical use[38]. As mentioned above, another popular method of replacing the hydrophobic layer with a hydrophilic one is ligand exchange, in which nitrosonium tetrafluoroborate is often used.

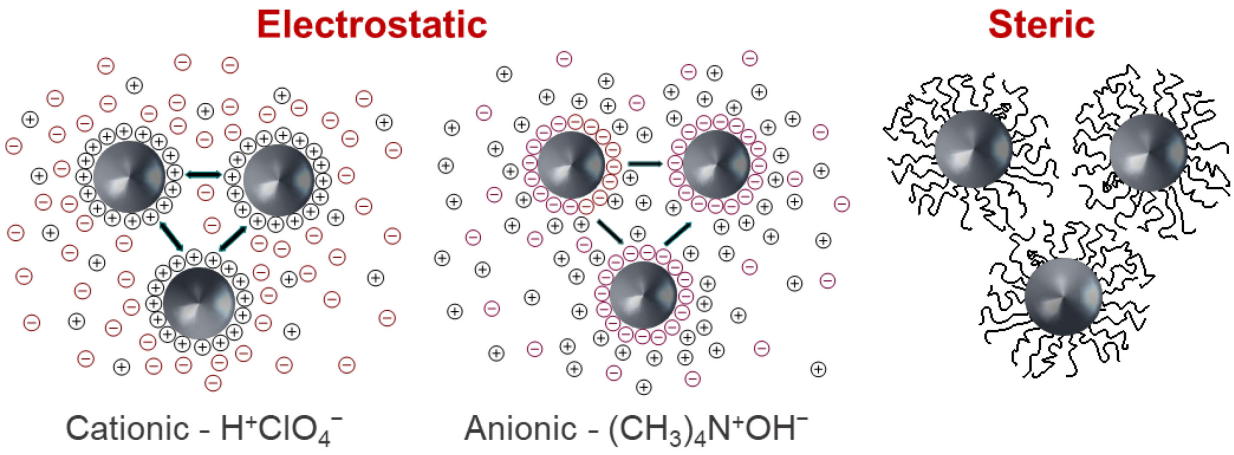

Figure 4. Electrostatic and steric stabilization of MNPs.

To bind macromolecules to the surface of MNPs, anchoring groups such as carboxylic acids, hydroxamates, phosphates, bisphosphonates, amino groups, thiol groups, aromatic vicinal diols, or silica, i.e. compounds capable of interacting with iron, are required[39]. Also, penta(propylene glycol)methacrylate phosphate (Sipomer PAM-200; hereafter referred to as SIPO) provides strong binding to iron due to the presence of a terminal phosphate group. SIPO is a heterobifunctional macromonomer consisting of five propylene oxide units and also a reactive methacrylic group, which can subsequently copolymerize with another monomer[40]. Another possible modification agent includes vinylidene diphosphonic acid.

1.5. Modification with antimicrobial agents

To achieve the microbicidal activity of MNPs to combat bacterial resistance, they were conjugated with various biocide agents like gentamicin[41] or silver which is known for its antifungal, antibacterial, anti-inflammatory and antiviral properties[42,43]. MNPs were also activated with β-cyclodextrin (β-CD), which is a macrocycle composed of seven glucose units.

Such an agent is suitable for the removal of drug residues from wastewater, cancer biomarkers from urine, or for hydrophobic drug delivery[44,45,46]. The ability of β-CD to generate different supramolecular structures and to incorporate guest molecules in its hydrophobic internal cavity was investigated, which enhanced the solubility and bioavailability of poorly soluble compounds. Several different strategies were applied for the preparation of β-CD-based antibacterial magnetic carriers for delivery of antibiotics, such as penicillin or ofloxacin[47,48]. To introduce biocidal properties, the MNPs were also covered with biocompatible antimicrobial polymers[49] containing quaternary pyridinium, ammonium, or phosphonium cations, which complex with negatively charged proteins of bacteria killing them. The antibacterial mechanism of the particles was explained by the formation of temporary pores or defects in the lipid bilayer that disrupt the ionic balance of the cells[50], the release of metal ions and the reactive oxygen species formation[51] (Figure 5). For example, thermoresponsive and mucoadhesive poly[2-(dimethylamino)ethyl methacrylate] (PDMAEMA) inhibited growth of bacteria, e.g., *Staphylococcus aureus* and *Escherichia coli*[52]. Other PDMAEMA applications involved drug and nonviral gene delivery[53], protein separation, water purification, etc. Also, hydrophobic poly(2-*tert*-butylaminoethyl methacrylate) (PTBAEMA) has been exploited in different antimicrobial applications, displacing Ca^{2+} or Mg^{2+} ions from the membrane of the bacteria[54]. Meanwhile, the *tert*-butylamine moieties of PTBAEMA did not even require to be quaternized to be an efficient bacteria killer. Other promising approaches for obtaining MNPs with antibacterial properties are the integration of ultra-small nanoparticles of heavy metals (silver), direct conjugation of antibiotics or the introduction of polycations on the particle surface. Three strategies were used in this work for the design and preparation of antibacterial MNPs: decoration with silver, attachment of a cationic polymer and utilization of sulfamethazine.

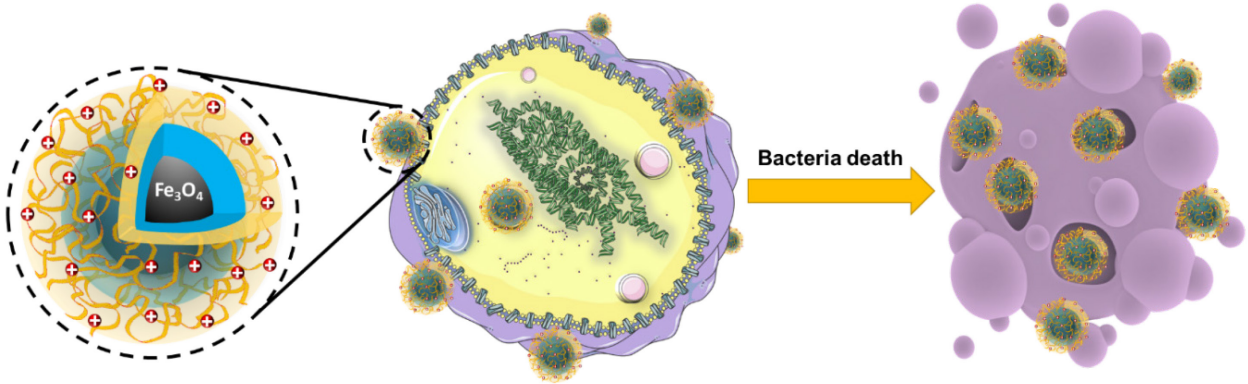

Figure 5. Schematic view of antibacterial activity of cation polymer-coated MNPs.

1.6. Use of MNPs with a focus on antibacterial applications

MNPs are very useful both in nanomedicine and also in industry, where they are used in magnetic inks, seals, lubricants, removal of heavy metals, bacteria and other contaminants from wastewater, desalination of seawater, catalysis in chemical reactions, and sensing of toxic gases, analytes and antibodies[55]. Biomedical applications of MNPs include two major areas, therapeutics and diagnostics, shortly termed as theranostics. In diagnostics, the external magnetic field targets and manipulates MNP-labeled proteins, cells and/or nucleic acids in biosensing, bioassays, and separation from biological media[56]. MNPs functionalized with specific antibodies or ligands that bind to bacterial pathogens aid in rapid and sensitive detection of bacterial infections. MNPs are also exploitable as contrast agents in MRI or magnetic particle imaging to early detect cancer and to monitor the progress of treatment in regenerative medicine[8,56]. In contrast, therapeutic applications include tissue repair, gene therapy, drug delivery and magnetic hyperthermia for treatment of tumors, etc.

Important applications of antibacterial iron oxide nanoparticles include the release of antibiotics or other therapeutic agents at the site of infection, thereby increasing the efficacy of the treatment while minimizing side effects[57]. Functionalized iron oxide nanoparticles incorporated into wound dressings provide a controlled release of antibacterial agents to promote healing and prevent infections[58]. Other functionalized MNPs capture bacteria to purify water for consumption or industrial use. Not only water purification, but also air filtration to capture airborne bacteria prevents the spreading of infectious diseases[59]. In addition, antibacterial MNPs can be used in food packaging to increase food safety and to extend shelf-life by inhibiting bacterial growth[60]. Antibacterial MNPs are also added to paints to create self-disinfecting coatings used in hospitals, public places and transportation to reduce the transmission of bacterial infections. Coatings containing antibacterial nanoparticles are also used in biomedical devices, catheters and implants, where they prevent bacterial colonization and thus reduce the risk of infections[61].

2. Aims

The aim of this thesis was to design, synthesize and characterize a biocompatible iron oxide-based magnetic carrier with superior antibacterial properties and colloidal stability. To achieve this goal, the particle surface was functionalized and decorated with silver nanoclusters or modified with water-soluble cationic polymers prepared by polymerization of DMAEMA and TBAEMA and/or with dextran and β-cyclodextrin to conjugate antibiotic silver-sulfamethazine. Another aim was to investigate the antimicrobial activity of the particles against *E. coli*, *S. aureus*, *C. albicans* and *A. niger*. The advantage of these new nanomaterials consists in their easy manipulability, targeting and separation from liquid media using a magnet, which makes them a suitable candidate for targeting bacterial infections.

The specific aims were as follows:

1. Synthesis of superparamagnetic maghemite (γ-Fe_2O_3) and magnetite (Fe_3O_4) nanoparticles with a narrow size distribution by
   - aqueous coprecipitation of Fe(II) and Fe(III) chlorides and
   - thermal decomposition of Fe(III) oleate.
2. Modification of the particle surface with biocompatible shells of
   - silica,
   - Sipomer PAM-200, PDMAEMA or PTBAEMA and
   - dextran/β-cyclodextrin.
3. Introduction of antibacterial moieties, such as silver and an antibiotic (silver-sulfamethazine) on the surface-modified MNPs.
4. Physicochemical characterization of the MNPs and *in vitro* investigation of their antimicrobial effect against Gram-positive and Gram-negative bacteria and fungi.

3. Experimental

3.1. Preparation of γ-Fe_2O_3 and Fe_3O_4 nanoparticles

Although different methods have been used to produce colloidally stable iron oxide nanoparticles of different sizes (1–100 nm), shapes and surface functionalization[32], the most commonly used techniques, such as coprecipitation of Fe salts and thermal decomposition of Fe organic precursor, were used in this dissertation. All chemicals employed below were from commercial sources, details are described in publications No. 1-3.

Coprecipitation of iron salts. Colloidal maghemite (γ-Fe_2O_3) was prepared by coprecipitation of aqueous Fe(II) and Fe(III) chlorides with ammonium hydroxide followed by oxidation of Fe_3O_4 with sodium hypochlorite[62]. Briefly, a solution of $FeCl_3 \times 6H_2O$ (5.406 g; 0.02 mol) in water (100 ml) and 25 % NH_4OH (100 ml, 0.05 mol) were sonicated for 5 min, a solution of $FeCl_2 \times 4H_2O$ (1.988 g, 0.01 mol) in water (50 ml) was added dropwise and the mixture sonicated. The mixture was added to NH_4OH (400 ml, 0.05 mol) and stirred with an anchor-type stirrer (300 rpm) at room temperature (RT) for 1 h. The resulting black precipitate was magnetically separated, washed with Q-water until peptization and sonicated with 5 wt.% NaOCl solution (16 ml) for 5 min. The precipitate was again magnetically separated and washed with Q-water until peptization accompanied by the formation of colloidal γ-Fe_2O_3 occurred.

Thermal decomposition of Fe(III) oleate. The preparation of Fe(III) oleate was carried out according to a previously published protocol[25]. Then, the mixture of Fe(III) oleate (5.76 g; 8 mmol), OA (0.3 mmol/ml) and OD (40 ml) was rapidly stirred (600 rpm) and preheated at 120 °C for 60 min under argon flow, which was followed by heating at 320 °C for 30 min. After colling to 70 °C, ethanol (100 ml) was added and the particles were separated using a magnet and subjected to three successive washes with hot ethanol (60–70 °C; 50 ml each) to remove residual solvents and OA. Finally, the Fe_3O_4 nanoparticles were dispersed in hexane and stored for subsequent use.

3.2. Synthesis of a functional shell on the particle surface

Advantageously, the surface of the γ-Fe_2O_3 or Fe_3O_4 particles contains hydroxyl groups that can be used to attach polymeric chains of organic (e.g., poly[2-(dimethylamino)ethyl methacrylate], poly[2-(*tert*-butylamino)ethyl methacrylate], functionalized dextran) or inorganic materials (e.g., silica). The modification methods used in this dissertation are described below.

Coating of MNPs with silica by reverse microemulsion technique. Silica was introduced on the OA-stabilized Fe_3O_4 particles by the water-in-hexane microemulsion via condensation of TMOS (see the publication No. 1). The mixture of Fe_3O_4 (40 mg), Igepal CO-520 (2 ml), hexane (38.4 ml) and 25 % NH_4OH (0.32 ml) was sonicated (Bandelin Sonopuls; Berlin, Germany; 10 % power) at RT for 30 min. After the addition of TMOS (0.04 ml), the reaction mixture was stirred (750 rpm) for 48 h. Then, MPTMS (0.02 ml) was added and the mixture was allowed to react at RT for 24 h to form Fe_3O_4@SiO_2-SH nanoparticles. Finally, acetone (15 ml) was added and the particles were washed with ethanol (30 ml, five times each) and water (30 ml, five times each) to remove residual surfactants.

Coating of MNPs with DMAEMA-based copolymers. First, MNPs were coated with SIPO. Briefly, a dispersion of Fe_3O_4 particles (0.2 g) in toluene (25 ml) and SIPO (0.4 g) was sonicated (20 % power) at RT for 5 min and then kept under argon atmosphere for 15 min, which was followed by stirring (900 rpm) at RT for 48 h. The resulting Fe_3O_4@SIPO particles were washed with hexane (100 ml, three times each) and dispersed in THF (5 ml). DMAEMA-based copolymers, namely PDMAEMA or P(DMAEMA-TBAEMA) obtained by 4,4'-azobis(4-cyanovaleric acid)-initiated free-radical polymerization, were grafted on the surface of Fe_3O_4@SIPO particles according to the procedure described in the publication No. 2.

Coating of MNPs with dextran/β-cyclodextrin. Functionalization of MNPs with DPA-Dex-β-CD polysaccharide was performed by multistep modifications of dextran and β-cyclodextrin.

Synthesis of 6-toluenesulfonyl-β-cyclodextrin (β-CD-Ts). Briefly, aqueous suspension (125 ml) of β-CD (5.75 g; 5 mmol) and Ts_2O (3.3 g; 10 mmol) was stirred at RT for 2 h. An aqueous solution of 0.125 M NaOH (25 ml) was added and after 10 min unreacted Ts_2O was filtered out (filter with 0.2 μm pores). The pH of the filtrate was adjusted to ~8 by the addition of NH_4Cl and the solution was kept at 4 °C for 16 h. The resulting β-CD-Ts precipitate was collected by filtration, washed with cold water and acetone and dried under vacuum (133 Pa).

Synthesis of 6-deoxy-6-hydroxyethylamino-β-cyclodextrin (β-CD-EA). The reaction mixture of β-CD-Ts (1.16 g; 0.9 mmol) and AE (2.72 ml; 45 mmol) in DMF (10 ml) was stirred (600 rpm) at 80 °C for 48 h. Subsequently, THF (100 ml) was added and β-CD-EA precipitate was filtered through a polytetrafluoroethylene membrane (0.5 μm pores), washed twice with THF (30 ml) and vacuum dried (133 Pa).

Synthesis of 6-deoxy-6-(2-hydroxyethyl) (vinylsulfonyl)methylamino-β-cyclodextrin (β-CD-VS). To an aqueous solution (8 ml) of β-CD-EA (1 g; 0.83 mmol) was added divinyl sulfone (0.2 ml; 2.07 mmol) and the reaction mixture was stirred (600 rpm) at RT for 2 h. The resulting β-CD-VS was precipitated in THF (80 ml), filtered off and dried in vacuo.

Synthesis of 6-toluenesulfonyl dextran (Dex-Ts). The mixture of anhydrous LiCl (3.0 g; 70.8 mmol) and dextran (5 g) in dimethylacetamide (125 ml) was stirred (600 rpm) at 80 °C for 3 h and then cooled to 8 °C. Subsequently, solutions of triethylamine (25.78 ml; 184.8 mmol) and TsCl (17.62 g; 92.4 mmol) in dimethylacetamide (24 ml each) were added dropwise and the mixture was allowed to react at 8 °C with stirring (400 rpm) for 36 h. The resulting Dex-Ts was precipitated two times in water (600 ml each) and dried at RT under vacuum (133 Pa).

Synthesis of 6-deoxy-6-hydroxyethylaminodextran (Dex-EA). The mixture of Dex-Ts (3 g) in DMF (30 ml) and EA (23.95 ml; 396 mmol) was kept under an argon atmosphere for 25 min and allowed to react at 90 °C for 48 h with constant stirring (600 rpm). Obtained Dex-EA was precipitated in THF two times (100 ml each), purified on a Sephadex® G-25 column, dialyzed against water using a cellulose dialysis membrane (MWCO = 12-14 kDa) for 48 h to remove excessive EA and finally lyophilized.

Modification of Dex-EA with β-CD-VS and functionalization with vinylidene 1,1-diphosphonic acid (VDPA). Briefly, a solution of Dex-EA (0.25 g) and β-CD-VS (0.78 g; 0.6 mmol) in water (25 ml) was stirred (800 rpm) at 37 °C for 24 h. Then, Dex-β-CD was dialyzed (MWCO = 12-14 kDa) against water for 72 h and lyophilized. The 1,1-diphosphonic acid-terminated β-cyclodextrin/dextran conjugate (DPA-Dex-β-CD) was prepared by adding an aqueous solution (1 ml) of VDPA (0.07 g; 0.38 mmol) at pH 10.8 adjusted by the addition of 10 M NaOH to an aqueous solution (8 ml) of Dex-β-CD (0.25 g); the mixture was then kept under stirring (800 rpm) at 50 °C for 24 h. The pH of the resulting DPA-Dex-β-CD was adjusted to 2 by the addition of 1 M HCl and the product was twice purified on a Sefadex G-25 column with water as eluent and lyophilized.

3.3. Attachment of biocide agents

Silver. Silver nanoclusters were introduced on the Fe_3O_4@SiO_2-SH particles by the reduction of silver nitrate with sodium borohydride. Briefly, 1 M $AgNO_3$ aqueous solution (0.05 ml) and 3 M aqueous NH_3 solution (0.15 ml) were added dropwise to the Fe_3O_4@SiO_2-SH colloid with sonication for 3 min and stirring (750 rpm) for 20 min; the $Ag(NH_3)^{2+}$ complex was formed. Subsequently, 2 M $NaBH_4$ aqueous solution (0.1 ml) was added dropwise and the

mixture was stirred for additional 1 h. The resulting Fe_3O_4@SiO_2-Ag nanoparticles were washed with ethanol and water five times each and dispersed in water.

Silver-sulfamethazine. SMT-Ag was conjugated on the γ-Fe_2O_3 particles by the following procedure. Briefly, γ-Fe_2O_3@DPA-Dex-β-CD particles were prepared by mixing an aqueous dispersion of MNPs (6 ml; 40 mg particles) with an aqueous solution (4 ml) of DPA-Dex-β-CD conjugate (40 mg) under sonication for 5 min and followed by stirring (800 rpm) at RT for 3 days. Then, γ-Fe_2O_3@DPA-Dex-β-CD particles were magnetically separated, washed with water three times (10 ml each) using centrifugation and redispersed in water (2 ml). The mixture of SMT-Ag (10 mg) in 0.06 % NH_4OH (10 ml) was sonicated for 5 min and added, the whole mixture was stirred (800 rpm) at RT for 3 days, and the resulting γ-Fe_2O_3@DPA-Dex-β-CD-SMT-Ag particles were washed as described above. More details can be found in the publication No. 3.

3.4. Characterization methods

The morphology, shape, size and particle size distribution were evaluated from approximately 400 particles in micrographs from a Tecnai G2 Spirit Twin 12 transmission electron microscope (TEM; FEI; Brno, Czech Republic); the number-average diameter (D_n), weight-average diameter (D_w) and dispersity ($Đ$) were calculated using Atlas software (Tescan; Brno, Czech Republic) according to equations 1-3:

$$D_n = \frac{\sum(n_i \cdot D_i)}{\sum n_i} \quad (1),$$

$$D_w = \frac{\sum(n_i \cdot D_i^4)}{\sum(n_i \cdot D_i^3)} \quad (2),$$

$$Đ = \frac{D_w}{D_n} \quad (3),$$

where n_i and D_i are the number and diameter of the i-th nanoparticle, respectively.

The hydrodynamic diameter (D_h), polydispersity (PD) and electrophoretic mobility (converted to ζ-potential) of the nanoparticles were obtained by dynamic light scattering (DLS) using a Zetasizer Ultra analyzer (Malvern Panalytical; Malvern, UK).

Weight-average molecular weight (M_w) of the polymers was determined by the size-exclusion chromatography (SEC) with a TSKgel SuperAW-L guard column (L × I.D. 4.6 mm × 3.5 cm, particle size 7 μm; Polymer Laboratories; Church Stretton, UK) and UVD 305 (Watrex; Prague, Czech Republic) and RI-101 (Shodex; Tokyo, Japan) detectors.

Methanol/acetate buffer (80/20 v/v) was used as the mobile phase at a flow rate of 0.5 ml/min; a polystyrene standard was used for the calibration. The molar mass was calculated using Clarity software (DataApex; Prague, Czech Republic).

All ^{1}H, ^{13}C and ^{31}P NMR spectra were recorded using a Bruker Avance III 600 spectrometer operating at 600.2 MHz and processed using Bruker TopSpin 4.1.1 software. The samples were dissolved either in deuterated dimethyl sulfoxide or D_2O at 295 K. ^{1}H 1D NMR spectra were obtained using a 90° pulse (width 18 μs) with a 10 s recycle delay and 16-64 number of scans. The diffusion of the components in the samples was investigated by pulsed-field gradient NMR using a 2D diffusion-ordered spectroscopy (DOSY) with a DiffBB diffusion probehead and 40 A gradient amplifiers. A double-stimulated echo pulse sequence was used to measure the self-diffusion coefficients *D*. The self-diffusion coefficients were obtained by least-squares fitting of the Stejskal-Tanner equation using Bruker Dynamics center 2.6.1 software. Chemical shifts were calibrated using hexamethyldisiloxane as an external standard.

Elemental analysis was determined using a Perkin-Elmer 2400 CHN elemental analyzer (Waltham, MA, USA). ATR-FTIR spectra were measured on a PerkinElmer Paragon 1000PC spectrometer using a Specac MKII Golden Gate single attenuated total reflection (ATR) system with a diamond crystal; the angle of incidence was 45°. A PerkinElmer 3110 atomic absorption spectrometer (AAS) was used to analyze the amount of iron and silver in the particles by measuring the solution obtained after mineralization with a mixture of 68 % $HClO_4$/65 % HNO_3 (4:1) at 80 °C for 20 min. XPS analyses were performed on a K-Alpha^{+} XPS spectrometer (ThermoFisher Scientific; East Greenstead, UK) at a pressure of 1.0×10^{-7} Pa. Magnetic properties of the nanoparticles were measured at RT using an EV9 vibrating magnetometer (DSM Magnetics ADE; Lowell, MA, USA) with the maximum magnetic field of 1 T.

The antibacterial activity of Fe_3O_4@SiO_2-Ag, Fe_3O_4@PDMAEMA and Fe_3O_4@P(DMAEMA-TBAEMA) nanoparticles was analyzed against Gram-positive *S. aureus* and Gram-negative *E. coli* bacteria cultivated on Luria agar (LA) plates or in Luria broth (LB) at 37 °C. For colony counts on LA, overnight cultures of *S. aureus* and *E. coli* were resuspended in phosphate-buffered saline, optionally Hank's balanced salt solution, and diluted in 1 or 2 ml of LB to 1×10^{5} or 10^{7} colony-forming units (CFU)/ml. Fe_3O_4@SiO_2-Ag, Fe_3O_4@PDMAEMA and Fe_3O_4@P(DMAEMA-TBAEMA) nanoparticles (5.5-175 μg/ml) were added to the cultures in six-well plates and incubated at 37 °C on a shaker (125 rpm). Cultures without nanoparticles were used as no treatment (NT) control and cultures with ampicillin (150 μg/ml) were used as positive control. After 0-4 h, aliquots were removed from the wells, diluted to 10^{-2}-10^{-6} for both

S. aureus and *E. coli*, seeded on LA plates and incubated at 37 °C for 24 h. Bacterial colonies were counted and CFU/ml was determined. Viability was calculated as the ratio of the number of living bacteria at a given time point to the number of living bacteria at time point 0. The procedure was repeated in three independent experiments in duplicates. In the case of nanoparticle coincubation with bacterial cultures in LB, sample turbidity was measured on a Synergy H1 Hybrid Reader (Biotek; Highland Park, VT, USA) at 600 nm and bacterial growth was evaluated by calculating viability (%) compared to NT control. The procedure was repeated in three independent experiments in duplicates. Statistical analysis was performed using GraphPad Prism5 software and one-way ANOVA test with Dunnett's multiple comparison test; the level of $P < 0.05$ was considered significant.

Disk diffusion test (DDT), minimum inhibitory and minimum bactericidal/microbicidal concentrations (MIC and MBC/MMC) were conducted to assess the bactericidal activity of γ-Fe_2O_3@DPA-Dex-β-CD-SMT-Ag particles. Filter paper disks (5 or 10 mm diameter; Whatmann Bio-Rad; Hercules, CA USA) were saturated with stock dispersions of particles (10 or 30 µl; 4 mg/ml) to achieve (40 or 120 µg) concentration per disk and dried at RT. Bacterial strains (*S. aureus* and *E. coli*) and *C. albicans* were prepared following the protocol recommended by EUCAST[63]. A 24-h yeast culture was standardized to 0.5 McFarland, while *A. niger* was subcultured on a Sabouraud dextrose agar plate (HiMedia; Mumbai, India) at 37 °C for 7 days and standardized similarly. Inoculum suspensions were spread evenly over Mueller–Hinton agar plates (Oxoid; Basingstoke, UK) and prepared disks were placed in triplicate on the agar surface. After static incubation, inhibition zones and growth were assessed. For MIC and MBC/MMC determination, the international ISO 20776-1 standard and EUCAST recommendations were followed. A quantitative microdilution broth assay was performed using 96-well microtiter plates. Particle concentrations ranging from 1,500 to 2.5 µg/ml were prepared and added to respective wells. After inoculation with microorganisms, plates were incubated at 37 °C for 18 h and growth was evaluated.

4. Results and discussion

4.1. Synthesis of MNPs and their physicochemical properties

Spherical Fe_3O_4 nanoparticles with a typical size of 16 nm were prepared by thermal decomposition of Fe(III) oleate and stabilized by oleic acid as described in my publications No. 1 and 2. A big advantage of this technique is that it allows the preparation of monodisperse magnetic nanoparticles (dispersity $Đ$ <1.05) of the same physicochemical and biological properties; moreover, the particles have high crystallinity and controlled size. The synthesis proceeded in three steps including a generation of poly(iron oxo) clusters, rapid nucleation and nanoparticle growth facilitated by increasing reaction temperature[64]. Since the size of nanoparticles can be regulated by changing the synthesis conditions such as reaction time and temperature, it is typically controlled by using different nonpolar high-boiling point organic solvents such as octadec-1-ene (OD) or icosane (IS)[25]. Smaller particles were produced in OD compared to the IS, since the former solvent had a lower boiling temperature in contrast to the latter one. Similarly, a shorter reaction time resulted in smaller particles as shown by TEM analysis (Figure 6 a-c). The monodispersity was achieved by a combination of short nucleation time and the presence of OA stabilizer, which prevents the aggregation of nuclei and ensures uniform conditions for the growth of each particle. The hydrodynamic diameter of the nanoparticles in hexane was slightly larger (D_h = 24-36 nm) than D_n due to the OA stabilizer adsorbed on the particle surface. Additionally, the polydispersity (PD = 0.01) documented a very narrow particle size distribution.

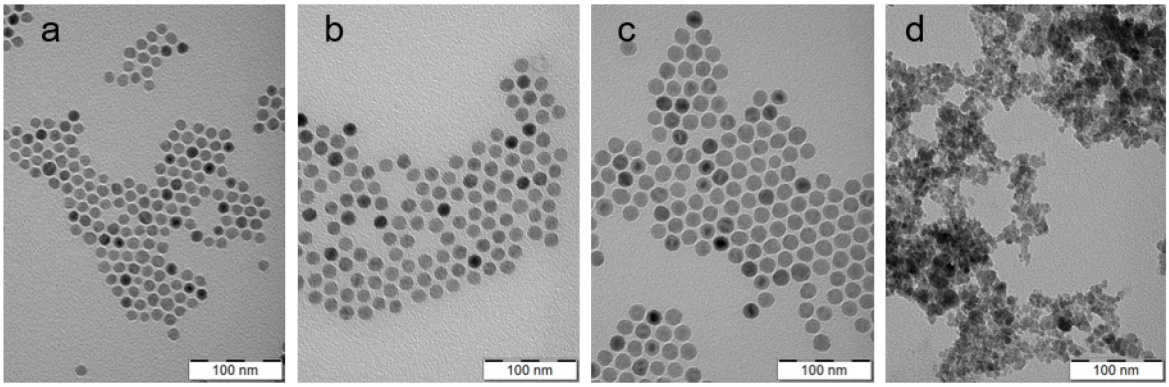

Figure 6. TEM micrographs; dependence of diameter of oleic acid-stabilized Fe_3O_4 nanoparticles prepared by thermal decomposition of Fe(III) oleate in octadec-1-ene at 320 °C on the reaction time. (a) 12-, (b) 16- and (c) 18-nm particles were synthesized for (a) 20, (b) 30 and (c) 40 min. (d) 9-nm γ-Fe_2O_3 nanoparticles prepared by coprecipitation of iron salts.

The chemical composition of the Fe_3O_4 nanoparticles was documented by both AAS and XPS spectroscopy. The high-resolution core level Fe 2p spectrum showed the presence of 41.3 wt.% of Fe, which was lower than the amount obtained from AAS (69.9 wt.%), because nanoparticles were coated with OA and XPS analyzes only up to an 8-nm thick layer of the sample. Another important parameter to prove the superparamagnetic character of the particles was the measurement of their magnetic properties, which are known to be governed by the size of iron oxide nanoparticles. Generally, particles <20 nm exhibit superparamagnetic properties at RT due to thermally induced spin flipping[21], which makes them colloidally stable and allows them to avoid magnetically driven aggregation, in contrast to ferro- and ferrimagnetic particles. At the same time, the superparamagnetic particles can be easily removed from aqueous suspensions using a magnet. Our Fe_3O_4 particles exhibited saturation magnetization M_s = 44.2 A·m^2/kg. With the exclusion of the diamagnetic oleate shell contribution, the M_s would reach 46 A·m^2/kg, which is significantly less than the saturation magnetization of bulk Fe_3O_4 (M_s = 92 A·m^2/kg)[65], nevertheless, it is comparable with reported values[66]. The variation may stem from the small particle diameter associated with the decrease in saturation magnetization. This reduction is ascribed to enhanced thermal fluctuation and a magnetically disordered surface, a consequence of the increased surface-to-volume ratio. Magnetic measurements of the Fe_3O_4 nanoparticles did not reveal any hysteresis loop (Figure 7). The absence of coercivity confirmed the superparamagnetic nature of the particles, indicating their non-interacting behavior.

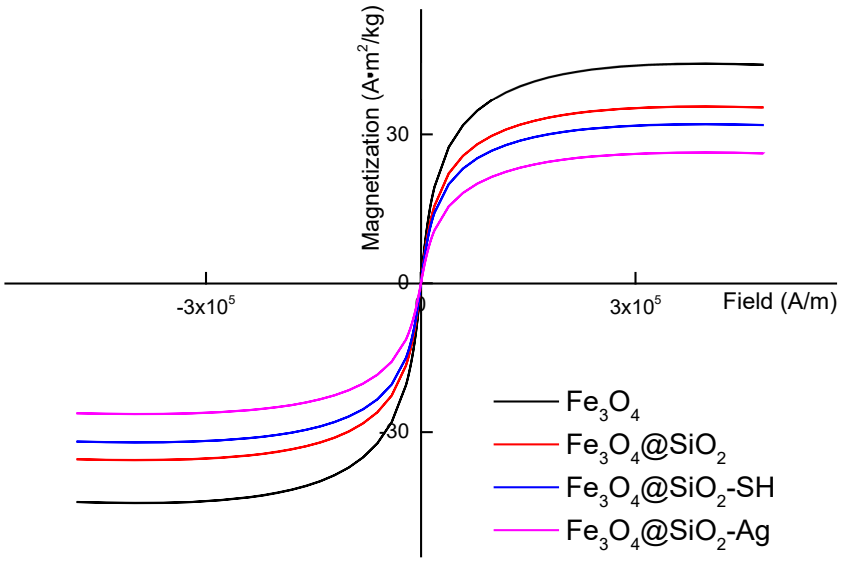

Figure 7. Magnetization curves of Fe_3O_4, Fe_3O_4@SiO_2, Fe_3O_4@SiO_2-SH, and Fe_3O_4@SiO_2-Ag nanoparticles.

Optionally, γ-Fe_2O_3 nanoparticles were obtained by coprecipitation of $FeCl_2$ and $FeCl_3$. Given that magnetite (Fe_3O_4) generated from the process is not chemically stable when exposed to air or water, a deliberate conversion into maghemite (γ-Fe_2O_3) through controlled oxidation with sodium hypochlorite was chosen. Subsequently, γ-Fe_2O_3 particles in their dehydrated state were examined using TEM. These γ-Fe_2O_3 particles exhibited a spherical-like morphology, with an average diameter of 8 nm and a dispersity of 1.29, indicating that the particles exhibited a broad size distribution (Figure 6 d). A larger D_h (108 nm) in water than D_n is typical for γ-Fe_2O_3 colloids, which can be attributed not only to partial aggregation but also to the presence of an electrical double layer surrounding the particles. Furthermore, DLS measures an intensity-weighted z-average diameter that is sensitive to large objects. The particles had negative ξ-potential amounting to -26 mV, which is a typical value for particles prepared by coprecipitation of $FeCl_2$ and $FeCl_3$ with a base[67]; this ensured the colloidal stability of the MNPs in water. More details can be found in the publication No. 3.

4.2. Silica-modified MNPs

The thermal decomposition method is characterized by providing hydrophobic Fe_3O_4 nanoparticles which, to be usable in a biological environment, must be hydrophilized in order to be transferred to an aqueous medium without aggregating. To do this, a ligand exchange technique is often used, but we modified the surface of the Fe_3O_4 particles with a silica (SiO_2) coating to achieve good colloidal stability in water[68]. Silica was coated on Fe_3O_4 particles using a water-in-hexane reverse microemulsion method that involved the hydrolysis and condensation of TMOS within the reverse micelles under NH_4OH catalysis (see my publication No. 1). The stabilization was achieved with Igepal CO-520 surfactant (Figure 8).

The relatively low TMOS/Fe_3O_4 particle weight ratio resulted in the production of core-shell nanoparticles with D_n = 21 nm and a thin silica shell measuring ~3 nm. Following the coating process, the hydrodynamic particle size in water increased to a larger value (D_h = 191 nm) due to the presence of the silica shell and particle clustering in water. Additionally, the presence of silica on the Fe_3O_4 particles was confirmed through XPS analysis, which revealed a decrease in the amount of Fe from 44.7 wt.% for the unmodified Fe_3O_4 nanoparticles to 14.5 wt.% for the Fe_3O_4@SiO_2 particles. This decrease was lower than that indicated by magnetic measurements (27.9 wt.%). The saturation magnetization M_s of Fe_3O_4@SiO_2 decreased to 35.5 $A \cdot m^2/g$ due to the contribution of the SiO_2 shell. The lower Fe content detected with XPS compared to magnetic measurements is expected, as the former is a surface-sensitive technique that measures only ~8 nm in depth.

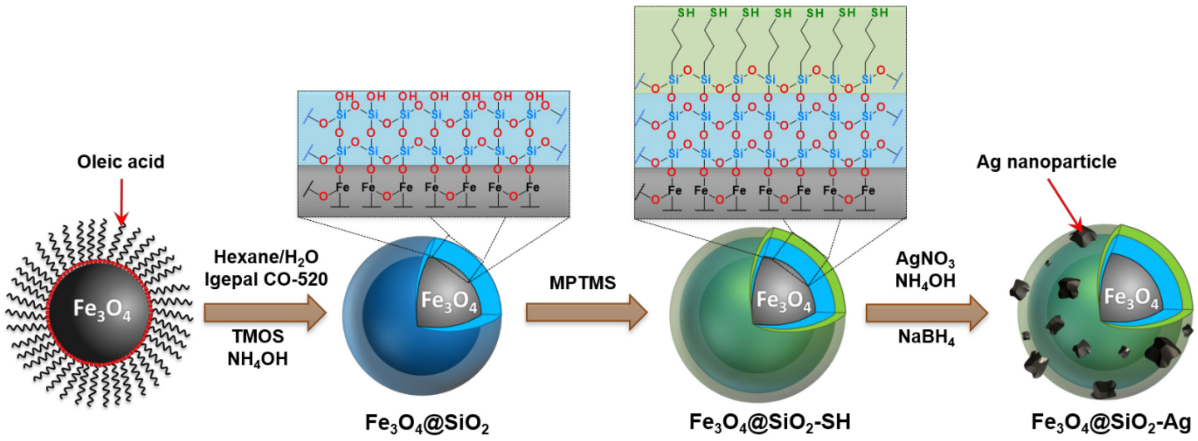

Figure 8. Scheme of surface modification of Fe_3O_4 nanoparticles with silica, (3-mercaptopropyl)trimethoxysilane (MPTMS) and decoration with silver. TMOS - tetramethyl orthosilicate.

MPTMS was utilized to introduce thiol groups onto the particle surface for potential silver attachment (Figure 8). The presence of the thiol groups was verified through elemental analysis, revealing a sulfur content of 3.6 wt.%. At the same time, the hydrodynamic diameter D_h increased to 210 nm (Table 1). The presence of SH groups on the Fe_3O_4@SiO_2-SH particles was corroborated by XPS analysis (Figure 9). The Fe content decreased from 14.5 wt.% in the Fe_3O_4@SiO_2 nanoparticles to 12.0 wt.% in the Fe_3O_4@SiO_2-SH particles. This decrease was attributed to the formation of a second thiol-containing silica layer following the addition of MPTMS during the sol-gel process. Magnetization measurements of the Fe_3O_4@SiO_2-SH particles indicated a saturation magnetization M_s of 32 A·m^2/g, corresponding to 25.2 wt.% of Fe (34.8 wt.% of Fe_3O_4).

4.2.1. Decoration of Fe_3O_4@SiO_2 nanoparticles with silver

Following the precipitation of $AgNO_3$ with sodium borohydride in the presence of Fe_3O_4@SiO_2-SH particles, silver nanoclusters were formed on the particle surface (Figure 8). The diameter of Fe_3O_4@SiO_2-Ag nanoparticles (D_n = 22 nm) remained almost the same as that in silica-modified particles. DLS, revealed an increase in the hydrodynamic particle size in water to 239 nm. The discrepancy between D_h values and D_n diameters calculated from TEM micrographs was explained already above.

The XPS analysis confirmed the decoration of Fe_3O_4@SiO_2-SH nanoparticles with silver (Figure 9). The Fe content decreased to 6.4 wt.% in the Fe_3O_4@SiO_2-Ag nanoparticles, attributed to the introduction of the silica shell and silver. The attachment of silver on the surface of Fe_3O_4@SiO_2-SH nanoparticles resulted in a reduction in the free thiol group content

to 2.9 wt.%. In comparison to Fe_3O_4 and Fe_3O_4@SiO_2 particles, the saturation magnetization of Fe_3O_4@SiO_2-Ag decreased to 26.3 A·m^2/kg, indicating the presence of diamagnetic silver on the particle surface. Consequently, the calculated Fe_3O_4 content was 28.6 wt.%, estimating the silver content to ~6 wt.%. Importantly, this additional coating did not affect the superparamagnetic behavior of the nanoparticles.

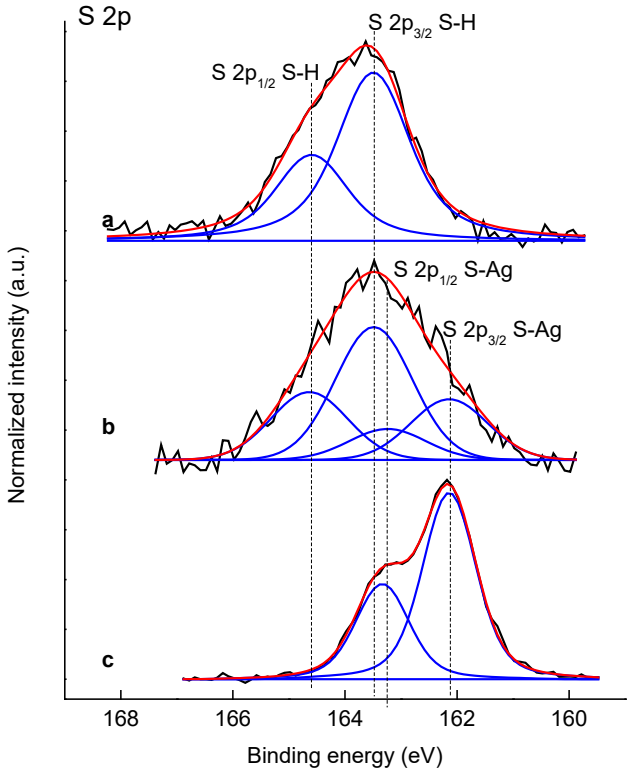

Figure 9. High resolution core level S 2p XPS spectra of (a) Fe_3O_4@SiO_2-SH, (b) Fe_3O_4@SiO_2-Ag and (c) reference 1-dodecanethiol self-assembled monolayer on a silver substrate. Spectra are depicted by black lines and the resulting fitted envelopes with red lines. The individual contributions of the fitted curve are shown with blue lines.

4.3. Modification of MNPs with SIPO, PDMAEMA and P(DMAEMA-TBAEMA)

Optionally, the Fe_3O_4 surface was functionalized using SIPO and cationic PDMAEMA and PTBAEMA (co)polymer, to enhance both particle dispersibility and colloidal stability in water. SIPO, terminated with phosphate group, was chosen as a mediator to ensure the effective attachment of both PDMAEMA and its copolymer to the iron oxide surface surpassing mere physical adsorption. The reactive methacrylic group of SIPO, featuring a vinyl bond separated by a ten-carbon spacer from the phosphate anchoring group, allowed for the free-radical copolymerization of the DMAEMA monomer[40]. Similar to OA, SIPO was not visible on the

TEM micrograph due to its low contrast. The hydrodynamic diameter of Fe_3O_4@SIPO in toluene only slightly decreased to 28 nm compared to the initial nanoparticles, possibly due to the less effective solvation of the SIPO shell in toluene compared to OA (Table 1).

Table 1. Physicochemical characterization of particles.

Particles	D_n (nm)	$Đ$	D_h (nm)	*PD*	ζ-potential (mV)	Coating[c] (wt.%)
Fe_3O_4	16	1.01	24[a]	0.01	-	-
γ-Fe_2O_3	8	1.29	108	0.13	-26	-
Fe_3O_4@SiO_2	21	1.02	191	0.25	-	-
Fe_3O_4@SiO_2-SH	21	1.04	210	0.14	-	-
Fe_3O_4@SiO_2-Ag	22	1.05	239	0.16	-	-
Fe_3O_4@SIPO	16	1.03	28[b]	0.16	-	8
Fe_3O_4@PDMAEMA	16	1.03	140	0.19	48	79
Fe_3O_4@P(DMAEMA-TBAEMA)	16	1.02	110	0.18	51	66
γ-Fe_2O_3@DPA-Dex-β-CD	9	1.28	155	0.07	-18	11
γ-Fe_2O_3@DPA-Dex-β-CD-SMT	8	1.26	244	0.29	-36	13

D_n - number-average diameter (TEM), $Đ$ - dispersity (TEM), D_h - hydrodynamic diameter by DLS in water ([a] in hexane, [b] in toluene), *PD* - polydispersity (DLS); [c] from TGA.

Among various antimicrobial polymers considered for coating MNPs, cationic PDMAEMA and PTBAEMA were chosen for their mucoadhesive, antibacterial, and stimuli-sensitive properties[52]. Due to limited solubility in water, TBAEMA was copolymerized with the highly hydrophilic DMAEMA monomer to form water-dispersible antibacterial magnetic agents. Initially, different DMAEMA/TBAEMA molar ratios were investigated in polymer preparation. MNPs coated with copolymers at a DMAEMA/TBAEMA ratio of 0.25/0.75 mol/mol were rather hydrophobic and non-dispersible in water. In contrast, Fe_3O_4@PDMAEMA and Fe_3O_4@P(DMAEMA-TBAEMA), prepared with DMAEMA/TBAEMA ratios of 1/0 and 0.75/0.25 mol/mol, respectively, were water-dispersible and thus selected for further experiments. The compositions of PDMAEMA and P(DMAEMA-TBAEMA) copolymers were analyzed using ^{1}H NMR spectroscopy by comparing methyl signals of side chains from DMAEMA and TBAEMA; the calculated monomer ratios in the (co)polymers were in good agreement with those added in the polymerization feed. The weight-average molecular weight M_w, number-average molecular

weight M_n, and polydispersity M_w/M_n of the polymers, determined by SEC analysis, indicated that with an increasing DMAEMA/TBAEMA ratio, the M_w of PDMAEMA and P(DMAEMA-TBAEMA) polymers increased from 145 kDa to 195 kDa, respectively. The polydispersity remained relatively low (M_w/M_n <1.2) due to polymer purification through dialysis and/or chromatography.

The colloidal stability of Fe_3O_4@PDMAEMA and Fe_3O_4@P(DMAEMA-TBAEMA) particles in water (pH 6) was proved through the determination of D_h and ζ-potential, reaching values of 140 and 110 nm and 48 and 51 mV, respectively (Table 1). At this pH, the amino groups of PDMAEMA were partially protonated, resulting in a relatively high ξ-potential. It is noteworthy that the hydrodynamic diameter D_h of particles tended to be larger than the number-average diameter D_n of dried particles obtained via TEM from the above described reasons. The extent of coating on the particles was determined by TGA, revealing 79 wt.% of PDMAEMA and 66 wt.% of P(DMAEMA-TBAEMA), including the contribution of SIPO (8 wt.%). This level of polymer coating proved sufficient to ensure robust colloidal stability even after one month of storage. Both types of nanoparticles were found stable at temperatures below 180 °C, meeting the requirements for prospective heat sterilization essential for biological experiments. More details can be found in the publication No. 2.

4.4. Modification of γ-Fe_2O_3 with dextran and silver-sulfamethazine-conjugated cyclodextrin

Considering antibiotics, sulfonamides exemplified by sulfamethazine (SMT) play an important role due to their low cost and widespread use in human medicine and agro-sector to treat different bacterial infections of the skin, lungs, ears and urinary tract[69]. The antibacterial effect of SMT, which was used in this dissertation, is based on competition with *p*-aminobenzoic acid involved in the enzymatic synthesis of dihydrofolic acid. Because sulfamethazine derivatives have limited solubility in water[70], SMT-Ag cannot be directly utilized *in vivo*. Thus, it is imperative to incorporate it into a hydrophilic carrier suitable for bioapplications. β-CD was selected as the carrier for SMT-Ag due to the presence of a hydrophobic pocket, facilitating easy loading of SMT and its derivatives[71]. In addition, β-CD was bound to Dex, which is a biocompatible, biodegradable, non-toxic and non-immunogenic polymer[72], making it a promising platform for the design of biosafe particles that are colloidally stable in water and body fluids. The synthesis of a reactive β-CD derivative, involved a three-step process: (*i*) tosylation of β-CD with Ts_2O in water followed by treatment with 10 % aqueous NaOH solution; (*ii*) reaction of β-CD-Ts with EA in DMF to yield β-CD-EA; and

(*iii*) introduction of reactive vinyl groups via an aza-Michael reaction with DVS to produce β-CD-VS. Simultaneously, the reaction of Dex with TsCl resulted in Dex-Ts, whose Ts groups were subsequently replaced with ethanolamine to form Dex-EA, which then underwent a reaction with the double bond of β-CD-VS, yielding Dex-β-CD (Figure 10). Finally, Dex-β-CD reacted with VDPA to produce DPA-Dex-β-CD.

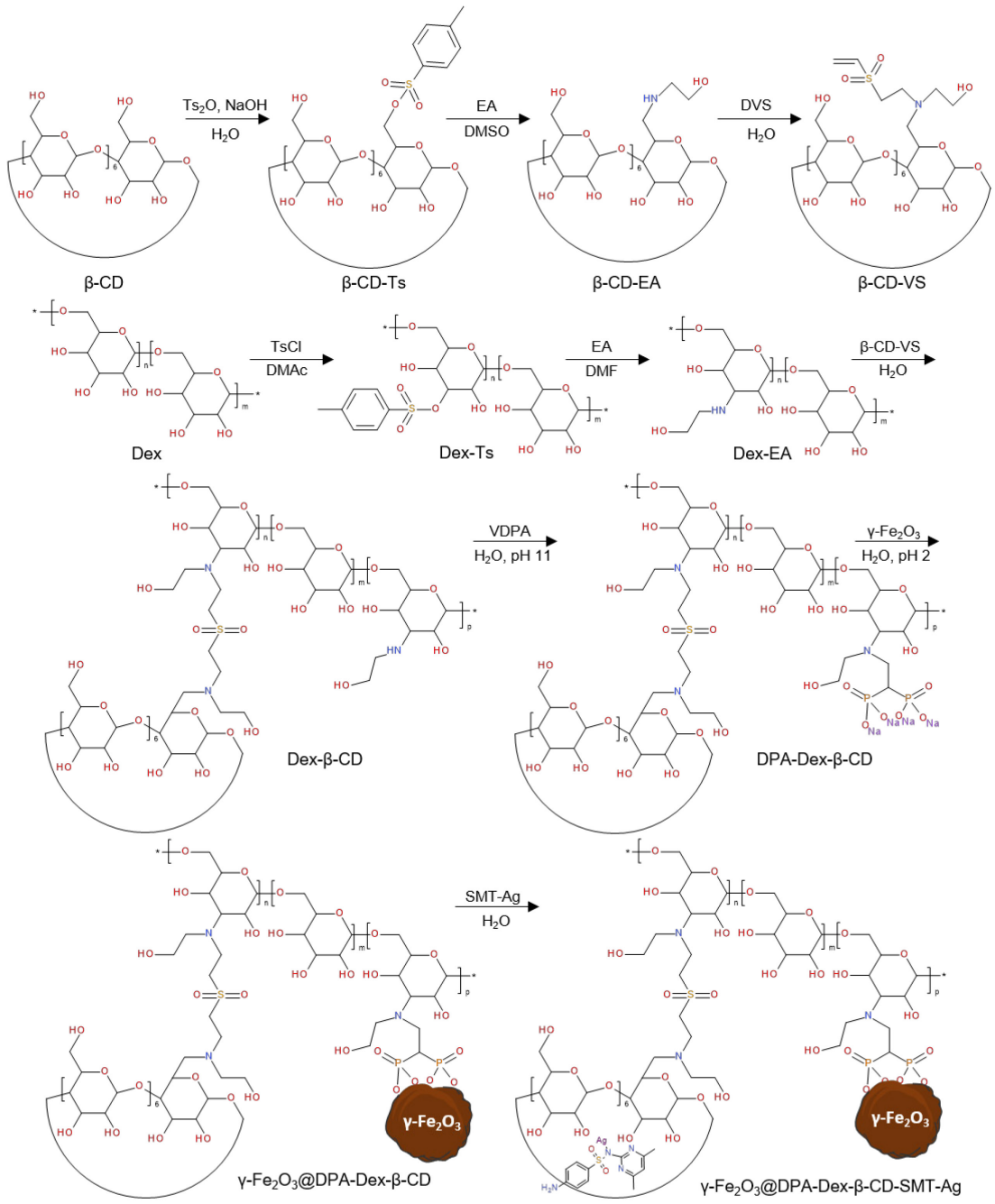

Figure 10. Synthesis of silver-sulfamethazine-conjugated β-cyclodextrin/dextran-coated magnetic nanoparticles (γ-Fe_2O_3@DPA-Dex-β-CD-SMT); DMSO - dimethyl sulfoxide, DMAc - *N,N*-dimethylacetamide, DMF - *N,N*-dimethylformamide, VDPA - vinylidene 1,1-diphosphonic acid.

The structure of prepared β-CD- and Dex-derivatives was confirmed by ATR-FTIR and ^{1}H, ^{13}C or ^{31}P NMR spectra. For example, in the ^{1}H NMR spectrum of Dex-Ts, by comparing the integral signal intensity from the C1 proton of Dex with the signals from the aromatic protons of the tosyl groups, it was found that, on average, 72 % of the glucose subunits of Dex have one hydroxyl group substituted by a tosyl group. The almost complete substitution of Ts groups by EA was confirmed by a corresponding ^{13}C NMR spectrum; based on the relative intensity of its signals, ~65 % of glucose units in Dex were modified with EA. In the case of the ^{1}H NMR spectrum of β-CD-Ts, its structure was confirmed by the presence of signals corresponding to methyl and aromatic protons from Ts which showed that, on average, one hydroxyl group of the β-CD ring was substituted by tosyl. To additionally confirm the chemical binding of Ts to β-CD, 2D NOESY and DOSY NMR spectra were recorded. Furthermore, the substitution of Ts groups of β-CD-Ts by EA was confirmed in the same way as in the case of Dex, i.e., from ^{1}H and ^{13}C NMR spectra. Also, the introduction of vinyl groups by the reaction of β-CD-EA with DVS was confirmed by the presence of signals from vinyl protons in the ^{1}H NMR spectrum of β-CD-VS. Moreover, diffusion NMR measurements showed the same self-diffusion coefficient of the VS group as that of the β-CD ring (1.01×10^{-10} m^2/s), indicating that VS was chemically bound to β-CD.

The analysis and precise identification of NMR signals in both ^{1}H and ^{13}C spectra for DPA-Dex-β-CD posed challenges due to the structural similarities between the subunits of modified Dex and β-CD, leading to signal overlap (Figure 11 a, b). Nevertheless, the formation of DPA-Dex-β-CD through the reaction of the β-CD-VS double bond with Dex-EA was inferred from the absence of NMR signals attributed to the VS groups. Furthermore, in the ^{13}C NMR spectrum of DPA-Dex-β-CD, distinct C1 carbon signals originating from both Dex and β-CD subunits were observed, providing further evidence of binding. Additionally, by comparing the integral C1 signal intensity of the β-CD carbon rings at 102.58 ppm with the C1 signals of the Dex main chain and terminal groups at 98.77 and 101.17 ppm, respectively, the approximate number of β-CD units in DPA-Dex-β-CD was determined, revealing that approximately 63 % of glucose units in Dex were bound to β-CD. Lastly, the ^{31}P NMR spectrum of DPA-Dex-β-CD exhibited a distinct signal at 11.2 ppm, corresponding to the diphosphonic acid groups (Figure 11 c).

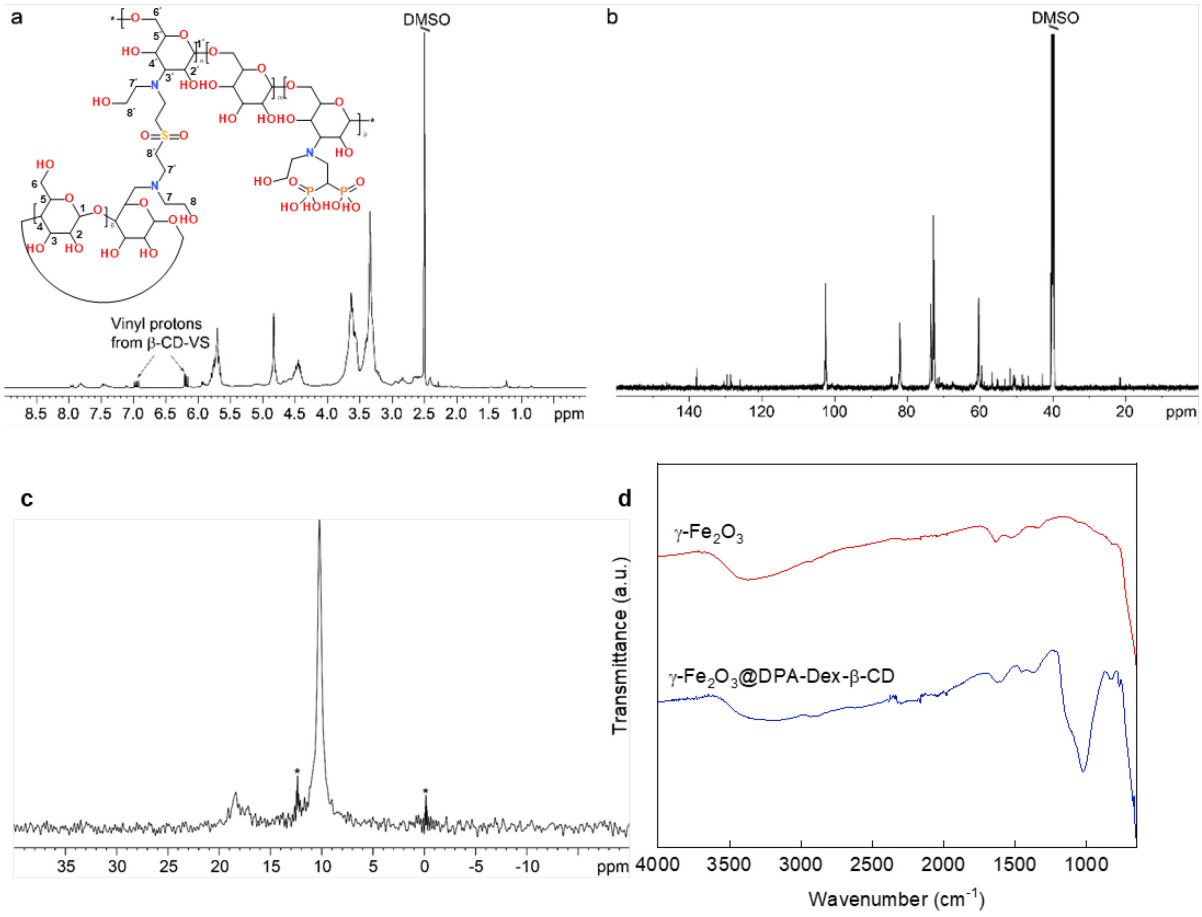

Figure 11. (a) ^{1}H NMR, (b) ^{13}C NMR and (c) ^{31}P NMR spectra of DPA-Dex-β-CD. (d) FTIIR spectra of γ-Fe_2O_3 and γ-Fe_2O_3@DPA-Dex-β-CD particles.

The incorporation of diphosphonic acid into the DPA-Dex-β-CD conjugate facilitated complexation with Fe ions of iron oxide, yielding stable water-dispersible particles in agreement with the literature[73]. In contrast to the neat particles, the FTIR spectrum of γ-Fe_2O_3@DPA-Dex-β-CD exhibited new peaks at 1,025 and 1,358 cm^{-1} that were assigned to ν_{as}(C-O-C) asymmetric and ν_s(CH_2) symmetric stretching vibration, respectively, which were characteristic of DPA-Dex-β-CD (Figure 11 d). According to the TGA, the γ-Fe_2O_3@DPA-Dex-β-CD particles contained 11 wt. % of the organic phase (Table 1). Hence, the FTIR spectroscopy and TGA confirmed the successful modification of the particle surface. Since the organic coating was not distinguishable in the TEM images, the number-average diameter and dispersity of γ-Fe_2O_3@DPA-Dex-β-CD remained comparable to pristine γ-Fe_2O_3 (Table 1). However, the hydrodynamic diameter of γ-Fe_2O_3@DPA-Dex-β-CD particles slightly increased (D_h = 155 nm) owing to the presence of the organic layer on the surface, with a small polydispersity (PD = 0.07), indicating a narrow size distribution. Upon mixing γ-Fe_2O_3@DPA-

Dex-β-CD particles with SMT-Ag, its complexation with β-CD occurred, resulting in the formation of γ-Fe_2O_3@DPA-Dex-β-CD-SMT-Ag particles (Figure 10). While their number-average diameter was nearly identical to that of the γ-Fe_2O_3@DPA-Dex-β-CD particles, the hydrodynamic diameter increased to 244 nm (*PD* = 0.29) due to the introduction of SMT-Ag. Contrary to γ-Fe_2O_3@DPA-Dex-β-CD particles, the thermogram of γ-Fe_2O_3@DPA-Dex-β-CD-SMT-Ag particles showed a 2 wt.% increase in organic content due to SMT-Ag incorporation (Table 1). Thus, the antibiotic content in the particles was estimated to ~29 μg per mg. The content of SMT-Ag incorporated into the particles was also quantified after their dissolution in hydrofluoric acid by UV-Vis spectroscopy amounting to 24 μg of antibiotic per mg of particles, which is a similar value to the TGA result. Full characterization of the γ-Fe_2O_3@DPA-Dex-β-CD-SMT-Ag particles was described in the publication No. 3.

4.5. Antibacterial activity of surface-engineered Fe_3O_4 and γ-Fe_2O_3 nanoparticles

Antibacterial properties of Fe_3O_4@SiO_2-Ag nanoparticles

Among various types of nanoparticles, including Al_2O_3, TiO_2, ZnO, NiO, CuO, and Ag, utilized against *E. coli*, *B. subtilis* and *S. aureus*, silver nanoparticles (<10 nm) are particularly recognized for their robust antibacterial properties[74,75]. While the precise mechanism behind the antimicrobial effects of silver is still under investigation, one potential impact involves the accumulation of nanoparticles on the cell surface, leading to the formation of pits and eventual bacterial death[76]. Interaction of silver nanoparticles with the bacterial surface can also generate free radicals, inducing oxidative stress and subsequent membrane damage[77]. Additionally, silver ions released from the nanoparticles can hinder the activity of crucial bacterial enzymes and impede the replication ability of bacterial DNA[78]. The antimicrobial efficacy of silver nanoparticles is influenced by various factors, including concentration, charge, morphology, exposure time, and notably, size and shape. Regarding morphology, triangular silver nanoplates and/or 10-12-nm particles exhibit higher efficiency compared to spherical or rod-like particles and/or larger particles due to their increased surface area[79].

To evaluate the antimicrobial activity of the monodisperse Fe_3O_4@SiO_2-Ag nanoparticles developed in this study, two experimental conditions were established. In both setups, Fe_3O_4@SiO_2 nanoparticles and no treatment control were utilized. *S. aureus* and *E. coli* were chosen in these experiments as model pathogens due to their differences in cell wall composition. Unlike *S. aureus*, *E. coli* features an additional outer membrane composed of proteins, phospholipids, and lipopolysaccharides, providing enhanced protection against

substances penetrating into the cytoplasm. Initially, bacterial colonies were exposed to the nanoparticles and subsequently counted on agar plates. In Figure 12, LB agar plates with both *S. aureus* and *E. coli* are presented, reflecting various incubation times (0-90 min) with Fe_3O_4@SiO_2-Ag particles at a relatively low concentration 50 µg/ml. Notably, Fe_3O_4@SiO_2-Ag nanoparticles exhibited an antibacterial effect against *S. aureus* (Figure 12 a-d). Analysis of the antibacterial activity of Fe_3O_4@SiO_2-Ag nanoparticles in the presence of *S. aureus* over 90 min revealed a significant decrease in viability after 30 and 60 min of incubation. On agar plates, the particles did not exhibit antibacterial activity against *E. coli* (Figure 12 e-h). The inhibitory effect on bacterial growth also demonstrated sensitivity to the initial number of cells in the experiment and the concentration of silver ions (see the publication No. 1). Importantly, the efficacy of antibacterial nanoparticles increased as the number of bacterial cells used in the experiment decreased, which is in agreement with a previous study[76].

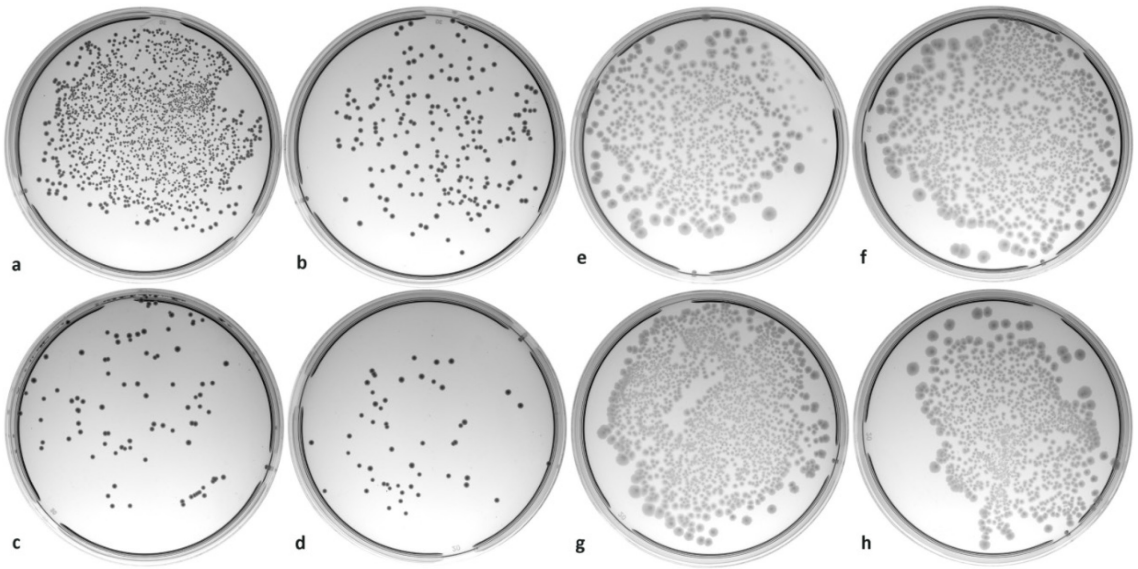

Figure 12. Agar plates were inoculated with suspensions of (a-d) *S. aureus* and (e-h) *E. coli*. Subsequently, the plates were incubated with Fe_3O_4@SiO_2-Ag nanoparticles (50 µg/ml) for (a, e) 0 min, (b, f) 30, (c, g) 60, and (d, h) 90 min.

In the second approach, the bacterial liquid culture was incubated with a serial dilution of Fe_3O_4@SiO_2 and Fe_3O_4@SiO_2-Ag nanoparticles, starting with a high concentration of 500 µg/ml, at 37 °C for 24 h; bacterial growth was assessed by measuring the culture turbidity. Untreated cells and cells treated with ampicillin served as controls. No notable inhibition of *E. coli* or *S. aureus* growth was observed after incubation with Fe_3O_4@SiO_2 particles. For *E. coli*, growth was significantly impeded after exposure to Fe_3O_4@SiO_2-Ag nanoparticles at

concentrations of 500 and 250 µg/ml, leading to a reduction in bacterial viability to 61 and 83 %, respectively. *S. aureus* viability was significantly affected starting from a concentration of 31.25 µg of Fe_3O_4@SiO_2-Ag/ml. Viability decreased to 73-88 % with particle concentrations ranging from 500 to 31.3 µg/ml, respectively. This is in agreement with previous studies suggesting that silver nanoparticles induce significant growth inhibition in *E. coli* while demonstrating only mild inhibition in *S. aureus*[80]. Additionally, it has been noted that free-radical generation is accompanied by subsequent membrane damage in Gram-negative *E. coli*. Studies have also reported the inhibition of *E. coli* growth by silver nanoparticles that accumulate both on the bacterial surface and inside the cells[76]. Further details on the antibacterial activity of Fe_3O_4@SiO_2-Ag particles can be found in my publication No. 1.

A comprehensive explanation of how nanoparticles penetrate the bacterial cell wall is not known. The cell wall of Gram-negative bacteria is comprised of lipoproteins, lipopolysaccharides, and phospholipids, forming a barrier that selectively permits the entry of only macromolecules[51]. In contrast, the cell wall of Gram-positive bacteria features a robust layer of peptidoglycan, along with teichoic acid and numerous pores that facilitate the penetration of foreign molecules, leading to cell membrane damage and eventual cell death[51]. The transport of 1-9 nm particles through porins has been proposed, influencing bacterial metabolism, such as oxidative stress[81]. Considering our 21-nm particles, rapid entry into the bacterial cell is unlikely. Instead, the accumulation of particles on the bacterial surface is believed to disrupt the cell wall, enabling subsequent infiltration of particles into the cytoplasm.

Antibacterial properties of cationic polymer-coated Fe_3O_4 nanoparticles

The antimicrobial efficacy of Fe_3O_4@PDMAEMA and Fe_3O_4@P(DMAEMA-TBAEMA) nanoparticles was again assessed against the Gram-positive *S. aureus* and the Gram-negative *E. coli*, both of which possess structurally distinct cell walls. Generally, positively charged nanoparticles are more effective against both Gram-positive and Gram-negative bacterial species than their negatively charged counterparts. The antibacterial mechanism of the cationic DMAEMA polymer and the hydrophobic TBAEMA polymer is believed to rely on electrostatic interactions between the cationic compound and the negatively charged cell surface, as well as hydrophobic interactions. This process involves penetration through the cell wall, binding to and disrupting the cytoplasmic membrane, ultimately leading to cell death. Moreover, Gram-negative bacteria generally require less charged and hydrophobic polymers to permeabilize the outer membrane.

The antimicrobial activity of Fe_3O_4@PDMAEMA and Fe_3O_4@P(DMAEMA-TBAEMA) particles (at concentrations of 5.5, 44, and 175 µg/ml) against both pathogens was assessed over a 0-4 h exposure period. The effects were observed to be concentration- and time-dependent. At the beginning of the experiment, the highest concentration of Fe_3O_4@P(DMAEMA-TBAEMA) particles (175 µg/ml) significantly reduced viability in both bacteria compared to Fe_3O_4@PDMAEMA. Higher concentrations of both particle types at the beginning decreased the viability of *E. coli* more than that of *S. aureus*. This trend persisted after 1 h of incubation. Conversely, a low concentration of nanoparticles (5.5 µg/ml) incubated for 4 h resulted in higher viability of *E. coli* than *S. aureus*, indicating a concentration-dependent effect (Figure 13). Furthermore, both particle types exhibited stronger antimicrobial activity after 1 h of incubation compared to the beginning of the experiment, suggesting a beneficial impact of prolonged bacterial exposure to nanoparticles for inducing cell wall damage. After 4 h of incubation, both Fe_3O_4@PDMAEMA and Fe_3O_4@P(DMAEMA-TBAEMA) particles significantly affected the viability of both Gram-positive and Gram-negative bacteria, reducing it to nearly zero (Figure 13).

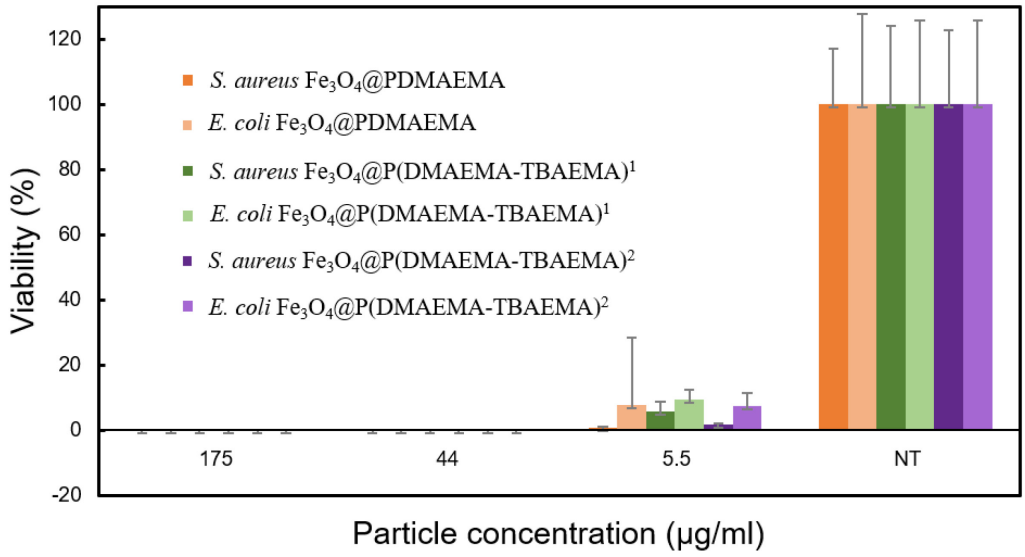

Figure 13. Viability of *S. aureus* and *E. coli* treated with Fe_3O_4@PDMAEMA and Fe_3O_4@P(DMAEMA-TBAEMA) particles for 4 h. Culture without any treatment (NT) served as a negative control. Data are expressed as mean ± standard deviation of bacterial viability relative to control in three independent experiments. The results denoted significant differences at $P < 0.001$ (two-way ANOVA with Bonferroni's test).

In summary, Fe_3O_4@PDMAEMA and Fe_3O_4@P(DMAEMA-TBAEMA) particles demonstrated potent bactericidal effects against both *E. coli* and *S. aureus*, with efficacy

dependent on the specific bacteria tested, particle concentration, time of incubation and coating. Notably, Fe_3O_4@P(DMAEMA-TBAEMA) particles exhibited particularly robust biocidal properties. For additional details, refer to my publication No. 2.

Antibacterial properties of Ag-SMT-conjugated γ-Fe_2O_3@DPA-Dex-β-CD-SMT nanoparticles

Sulfamethazine is a common antibiotic for treating Gram-positive bacterial infections, including staphylococcal infections (respiratory and urinary tracts) in humans and animals. DDT, a standard method endorsed by regulatory authorities (e.g., EUCAST, Clinical and Laboratory Standards Institute or Association of Official Agricultural Chemists), assesses the antimicrobial efficacy of compounds, including pharmaceuticals and disinfectants. Typically, a screening phase evaluates newly synthesized or naturally occurring molecules for antimicrobial potential. EUCAST-based methods rely on microbial physiology, evaluating inhibition zones for bacteria (*S. aureus* and *E. coli*) within a 24-h growth span and 72 h for mold (*A. niger*) to develop mature hyphal growth. The goal is to identify promising molecules for subsequent quantitative tests like minimum inhibitory concentration (MIC), minimum microbicidal concentration (MMC), and toxicity assessments. Our DDT findings revealed limited activity of γ-Fe_2O_3@DPA-Dex-β-CD-SMT-Ag particles against *S. aureus*, *E. coli*, and *A. niger*, with small inhibition zones (~1–2 mm). Obviously, the colloidal nature of the particle dispersions restricted the diffusion of their active ingredient (Table 2). This was evident in a complementary experiment with free SMT solution, showing inhibition zones around disks due to good diffusion of SMT. Particle dispersion with free SMT exhibited activity against *S. aureus*, while neat γ-Fe_2O_3 and γ-Fe_2O_3@DPA-Dex-β-CD particles showed no antimicrobial activity, confirming thus the observed inhibition effect was attributed to the encapsulated active compound (SMT-Ag).

Since DDT offered only qualitative insight into antibacterial activity, the MIC/MBC/MMC assay was selected to quantify the effect. MIC, a key quantitative measure of antimicrobial potential, denotes the lowest concentration inhibiting microbe growth under standard conditions (e.g., according to EUCAST). However, the MIC test itself does not distinguish between static (temporary growth inhibition) and cidal effects (complete devitalization of cells); these can be determined by MBC/MMC experiments. While γ-Fe_2O_3@DPA-Dex-β-CD-SMT-Ag particles exhibited good antibacterial effect against *S. aureus* and *E. coli* according to the MIC/MBC tests, the antifungal activity against *C. albicans* and *A. niger* was even more pronounced. This enhanced antibacterial action could be beneficial,

particularly in medical settings to combat *C. albicans* biofilms, common in hospital-acquired fungal infections. Notably, the lowest concentration inhibiting microorganism growth for γ-Fe_2O_3@DPA-Dex-β-CD-SMT-Ag particles was relatively high (500/1,000 μg/ml; Table 2). After recalculation, this means that the MIC/MBC for SMT-Ag was 12/24 μg/ml, which represents a higher antimicrobial activity than in previously published work[69]. In the agriculture and food industry, Ag nanoparticles (6-12 nm) are often effective at 400 mg/l, though 4-16 mg/l can suffice. For antifungal activity, MIC/MMC levels were 250/1,000 μg/ml (Table 2). Thus, the antimicrobial effect of Ag in the particles is most likely responsible for the antifungal activity, while SMT likely contributes to antibacterial action, particularly against *S. aureus*. However, no additive contribution from combined SMT-Ag was observed, possibly due to steric effects. Since fungal cells are larger than *S. aureus* or *E. Coli* and form hyphal structures, their surface area exposed to biocide-conjugated particles is greater. It is supposed that the mechanism of the antimicrobial effect of Ag involves breaking down the microbial cell wall structure, allowing ions (or other agents bound to the particles) to penetrate into the cells[82].

Table 2. Qualitative and quantitative evaluation of antimicrobial activity of nanoparticles.

Pathogen	*Staphylococcus aureus* CCM 2022		*Escherichia coli* CCM 3954		*Candida albicans* CCM 8186		*Aspergillus niger*	
Test / Particles	DDT	MIC/ MBC	DDT	MIC/ MBC	DDT	MIC/ MMC	DDT	MIC/ MMC
γ-Fe_2O_3	Growth around the disk/NT	NE/ NE	Growth around the disk/NT	NT	Growth around the disk/growth within the drop	NT	Growth around the disk/NT	NT
γ-Fe_2O_3@ DPA-Dex-β-CD	Growth around the disk/NT	NE/ NE	Growth around the disk/NT	NT	Growth around the disk/growth within the drop	NT	Growth around the disk/NT	NT
γ-Fe_2O_3@ DPA-Dex-β-CD-SMT-Ag	2-mm inhibition zone/no growth within the drop	500/ NE	1-mm inhibition zone/no growth within the drop	500/ 1,000	Growth around the disk/growth within the drop	250/ NE	2-mm inhibition zone/no growth within the drop	250/ 1,000

DDT - disk diffusion test (40 μg of particles, i.e., 10 μl drop on 5 mm disk); MIC/MBC/MMC - minimum inhibitory, bactericidal and microbicidal concentrations (μg/ml); NT - not tested; NE - not effective within the tested range of concentration (2.5-1,500 μg/ml).

5. Conclusions

Antibiotic resistance to bacteria is currently a major problem that could have a catastrophic impact on humanity in the future. Therefore, basic research is extremely important to advance innovative approaches to overcome these problems. In this respect, nanotechnologies, including nanomedicine, hold great promise in the fight against pathogen resistance. In this thesis, I have investigated the development of novel biocompatible iron oxide-based MNPs with antibacterial properties. At the same time, I paid attention to the good colloidal and chemical stability of the particles. The multistep approach to particle synthesis and surface functionalization strategies of MNPs were tailored to ensure that the particles effectively suppress bacterial infections while mitigating the undesirable side effects associated with the use of conventional antibiotics. For these tasks, I intentionally selected superparamagnetic nanoparticles because they can efficiently deliver the bactericidal agent to the site of infection using a magnetic field without the particles having side effects on healthy tissue; after the magnet is removed, the particles are again easily dispersible in water. Compared to the coprecipitation method, a major advantage of the thermal decomposition approach also used in this work is that it allows the morphology, size and shape of the particles to be tailored. Importantly, the particles are uniform in size, which ensures reproducibility of results, the same physicochemical and biological properties and easy manipulation. In addition, surface chemistry of MNPs was an integral part of my work, because not only did the polymer coating provide colloidal stability in aqueous media, but the presence of reactive functional groups also allowed the binding of the target agent (e.g., silver or silver-sulfamethazine). In the thesis, I focused on three different formulations of MNPs based on superparamagnetic Fe_3O_4 nanoparticles coated with silver-decorated silica, MNPs coated with cationic polymers and a magnetically controlled silver-sulfamethazine-based antibiotic delivery system. In particular, the latter formulation showed superior *in vitro* antibacterial efficacy against both Gram-positive (*S. aureus*) and Gram-negative (*E. coli*) bacteria, as well as antifungal activity against *C. albicans* and *A. niger*. This may be advantageous for the topical delivery of antimicrobial agents to treat bacterial or fungal infections in hospitals, prospectively in animals and possibly in humans.

However, let us note that further work is needed in this area to elucidate the mechanisms underlying the antimicrobial activity of MNP formulations, including their interactions with bacterial cell membranes and intracellular targets. Such mechanistic insights will facilitate the rational design of new generations of MNPs with enhanced specificity and efficacy against

antibiotic-resistant pathogens and reduce the risk of side effects associated with conventional treatments. When considering the applicability of the developed antimicrobial MNPs, we must not forget that they can be monitored in MRI, which would allow real-time monitoring of therapeutic intervention and/or disease progression. Last but not least, the easy magnetic separation of MNPs from liquids using an external magnetic field allows the reuse of particles, e.g. in wastewater disinfection. However, disinfection of food packaging or surfaces of medical instruments and devices contaminated with antibiotic-resistant pathogenic bacteria remains the main application outcome of the antibacterial magnetic nanoparticles we have developed.

6. References

1. Antibiotic resistance threats in the United States, U.S. Centers for Disease Control and Prevention (2019). doi:10.15620/cdc:82532

2. Alanis A.J., Resistance to antibiotics: Are we in the post-antibiotic era? Arch. Med. Res. 36, 697–705 (2005). doi:10.1016/j.arcmed.2005.06.009

3. Tagliabue A., Rappuoli R., Changing priorities in vaccinology: Antibiotic resistance moving to the top, Front. Immunol. 9, 1068 (2018) doi:10.3389/fimmu.2018.01068

4. Santos A.S., Ramalho P., Viana A.T., Lopes A.R., Gonçalves A.G., Nunes O.C., Pereira F.R., Soares S., Feasibility of using magnetic nanoparticles in water disinfection, J. Environ. Manag. 288, 112410 (2021). doi:10.1016/j.jenvman.2021.112410

5. Guo N., Cang F., Wang Z., Zhao T., Song X., Farris S., Li Y., Fu Y., Magnetism and NIR dual-response polypyrrole-coated Fe_3O_4 nanoparticles for bacteria removal and inactivation, Mater. Sci. Eng. C 126, 112143 (2021). doi:10.1016/j.msec.2021.112143

6. Fatima F., Siddiqui S., Khan W.A., Nanoparticles as novel emerging therapeutic antibacterial agents in the antibiotics resistant era, Biol. Trace Elem. Res. 199, 2552–2564 (2021). doi:10.1007/s12011-020-02394-3

7. Ali A., Shah T., Ullah R., Zhou P., Guo M., Ovais M., Tan Z., Rui Y., Review on recent progress in magnetic nanoparticles: Synthesis, characterization, and diverse applications, Front. Chem. 9, 629054 (2021). doi:10.3389/fchem.2021.629054

8. Gupta A.K., Gupta M., Synthesis and surface engineering of iron oxide nanoparticles for biomedical applications, Biomaterials 26, 3995–4021 (2005). doi:10.1016/j.biomaterials.2004.10.012

9. Yang X., Ren H., Li J., Sun B., Lu D., Li S., Zhang Y., Multifunctional $ZnFeO_4$-based antibiotic cross-linked nanoplatform for magnetically targeted treatment of microbial biofilms, CS Appl. Nano Mater. 6, 2141–2150 (2023). doi:10.1021/acsanm.2c05210

10. de Toledo L.A.S., Rosseto H.C., Bruschi M.L., Iron oxide magnetic nanoparticles as antimicrobials for therapeutics, Pharm. Dev. Technol. 23, 316–323 (2018). doi:10.1080/10837450.2017.1337793

11. Vallet-Regí M., González B., Izquierdo-Barba I., Nanomaterials as promising alternative in the infection treatment, Int. J. Mol. Sci., 20, 3806 (2019). doi:10.3390/ijms20153806

12. Sivula K., Le Formal F., Grätzel, M., Solar water splitting: Progress using hematite (α-Fe_2O_3) photoelectrodes, Chem. Sus. Chem. 4, 432–449 (2011). doi:10.1002/cssc.201000416

13. Sharma P., Umar A., Rana D.S., Kumar R., Chauhan S., Chauhan M.S., Growth and characterization of α-Fe_2O_3 nanoparticles for environmental remediation and chemical sensor applications, Sci. Adv. Mater. 7, 2747–2754 (2015). doi:10.1166/sam.2015.2709

14. Boxall C., Kelsall G., Zhang Z., Photoelectrophoresis of colloidal iron oxides. Part 2.—Magnetite (Fe_3O_4), J. Chem. Soc., Faraday Trans. 92, 791–802 (1996). doi:10.1039/FT9969200791

15. Wu W., Wu Z., Yu T., Jiang C., Kim W-S., Recent progress on magnetic iron oxide nanoparticles: synthesis, surface functional strategies and biomedical applications, Sci. Technol. Adv. Mater. 16, 023501 (2015). doi:10.1088/1468-6996/16/2/023501

16. Magnetic Nanoheterostructures: Diagnostic, Imaging and Treatment, Book Series: Nanomedicine and Nanotoxicology, ed. Sharma S.K., Javed Y., Springer (2020). doi:/10.1007/978-3-030-39923-8

17. Callister W.D. and Rethwisch D.G., Material Science and Engineering: An Introduction (7th edition), John Wiley & Sons, New York, USA (2006).

18. Kianfar E., Magnetic nanoparticles in targeted drug delivery: A review, J. Supercond. Nov. Magn. 34, 1709–1735 (2021). doi:10.1007/s10948-021-05932-9

19. Knobel M., Nunes W.C., Socolovsky L.M., De Biasi E., Vargas J.M., and Denardin J.C., Superparamagnetism and other magnetic features in granular materials: A review on ideal and real systems, J. Nanosci. Nanotechnol. 8, 2836–2857 (2008). doi:10.1166/jnn.2008.15348

20. Ghazanfari M.R., Kashefi M., Shams S.F., and Jaafari M.R., Perspective of Fe_3O_4 nanoparticles role in biomedical applications, Biochem. Res. Int. 7840161 (2016). doi:10.1155/2016/7840161

21. Baumgartner J., Bertinetti L., Widdrat M., Hirt A.M., Faivre D., Formation of magnetite nanoparticles at low temperature: From superparamagnetic to stable single domain particles, PLoS One 8, e57070 (2013). doi:10.1371/journal.pone.0057070

22. Ogbezode J.E., Ezealigo U.S., Bello A., Anye V.C., Onwualu A.P., A narrative review of the synthesis, characterization, and applications of iron oxide nanoparticles, Discover Nano 18, 125 (2023). doi:10.1186/s11671-023-03898-2

23. Wu W., He Q., Jiang C., Magnetic iron oxide nanoparticles: Synthesis and surface functionalization strategies, Nanoscale Res. Lett. 3, 397–415 (2008). doi:10.1007/s11671-008-9174-9

24. Hufschmid R., Arami H., Ferguson R.M., Gonzales M., Teeman E., Brush L.N., Browning N.D., Krishnan K.M., Synthesis of phase-pure and monodisperse iron oxide nanoparticles by thermal decomposition, Nanoscale 7, 11142–11154 (2015). doi:10.1039/c5nr01651g

25. Patsula V., Petrovský E., Kovářová J., Konefal R., Horák D., Monodisperse superparamagnetic nanoparticles by thermolysis of Fe(III) oleate and mandelate complexes, Colloid. Polym. Sci. 292, 2097–2110 (2014). doi:10.1007/s00396-014-3236-6

26. Kwon S.G., Piao Y., Park J., Angappane S., Jo Y., Hwang N.M., Park J.G., and Hyeon T., Kinetics of monodisperse iron oxide nanocrystal formation by "heating-up" process, J. Am. Chem. Soc. 129, 12571–12584 (2007). doi:10.1021/ja074633q

27. Guo J., Yang W., Wang C., Magnetic colloidal supraparticles: Design, fabrication and biomedical applications, Adv. Mater. 25, 5196-5214 (2013). doi:10.1002/adma.201301896

28. Lu A.-H., Salabas E.L., Schüth F., Magnetic nanoparticles: Synthesis, protection, functionalization, and application, Angew. Chem. 46, 1222–1244 (2007). doi:10.1002/anie.200602866

29. Dadfar S.M., Roemhild K., Drude N.I., von Stillfried S., Knüchel R., Kiessling F., Lammers T., Iron oxide nanoparticles: Diagnostic, therapeutic and theranostic applications, Adv. Drug Delivery Rev. 138, 302–325 (2019). doi:10.1016/j.addr.2019.01.005

30. Ramimoghadam D., Bagheri S., Hamid S.B.A., Progress in electrochemical synthesis of magnetic iron oxide nanoparticles, J. Magn. Magn. Mater. 368, 207–229 (2014). doi:10.1016/j.jmmm.2014.05.015

31. Khan A.A., Khan S., Khan S., Rentschler S., Laufer S., Deigner H.-P., Biosynthesis of iron oxide magnetic nanoparticles using clinically isolated *Pseudomonas aeruginosa*, Sci. Rep. 11, 20503 (2021). doi:10.1038/s41598-021-99814-8

32. Laurent S., Forge D., Port M., Roch A., Robic C., Elst L.V., Muller R.N., Magnetic iron oxide nanoparticles: Synthesis, stabilization, vectorization, physicochemical characterizations, and biological applications, Chem Rev. 108, 2064–2110 (2008). doi:10.1021/cr068445e

33. Rarokar N., Yadav S., Saoji S., Bramhe P., Agade R., Gurav S., Khedekar P., Subramaniyan V., Wong L.S., Kumarasamy V., Magnetic nanosystem a tool for targeted delivery and diagnostic application: Current challenges and recent advancement, Int. J. Pharm.: X 7, 2590–1567 (2024). doi:10.1016/j.ijpx.2024.100231

34. Horák D., Babič M., Jendelová P., Herynek V., Trchová M., Pientka Z., Pollert E., Hájek M., Syková E., *D*-Mannose-modified iron oxide nanoparticles for stem cell labeling, Bioconjugate Chem. 18, 635–644 (2007). doi:10.1021/bc060186c

35. Ruiz A., Morais P.C., de Azevedo R.B., Lacava Z.G.M., Villanueva A., del Puerto Morales M., Magnetic nanoparticles coated with dimercaptosuccinic acid: Development, characterization, and application in biomedicine, J. Nanopart. Res. 16, 2589 (2014). doi:10.1007/s11051-014-2589-6.

36. Mylkie K., Nowak P., Rybczynski P., Ziegler-Borowska M., Polymer-coated magnetite nanoparticles for protein immobilization, Materials (Basel) 14, 248 (2021). doi:10.3390/ma14020248.

37. Zhu N., Ji H., Yu P., Niu J., Farooq M.U., Akram M.W., Udego I.O., Li H., Niu X., Surface modification of magnetic iron oxide nanoparticles, Nanomaterials 8, 810 (2018). doi:10.3390/nano8100810

38. Tassa C., Shaw S.Y., Weissleder R., Dextran-coated iron oxide nanoparticles: A versatile platform for targeted molecular imaging, molecular diagnostics, and therapy, Acc. Chem. Res. 18, 842–852 (2011). doi:10.1021/ar200084x

39. Portet D., Denizot B., Rump E., Lejeune J.-J., Jallet P., Nonpolymeric coatings of iron oxide colloids for biological use as magnetic resonance imaging contrast agents, J. Colloid Interface Sci. 238, 37–42 (2001). doi:10.1006/jcis.2001.7500

40. Tocchio A., Horák D., Babič M., Trchová M., Veverka M., Beneš M. J., Šlouf M., Fojtík A., Magnetic poly(glycidyl metha-crylate) particles prepared in the presence of surface-modified γ-Fe_2O_3, J. Polym. Sci. 47, 4982–4994 (2009). doi:10.1002/pola.23551

41. Bhattacharya P., Neogi S., Gentamicin coated iron oxide nanoparticles as novel antibacterial agents, Mater. Res. Express 4, 095005 (2017). doi:10.1088/2053-1591/aa8652

42. Prucek R., Tuček J., Kilianová M., Panáček A., Kvítek L., Filip J., Kolář M., Tománková K., Zbořil R., The targeted antibacterial and antifungal properties of magnetic nanocomposite of iron oxide and silver nanoparticles, Biomaterials 32, 4704–4713 (2011). doi:10.1016/j.biomaterials.2011.03.039

43. Durán N., Durán M., de Jesus M.B., Seabra A.B., Fávaro W.J., Nakazato G., Silver nanoparticles: A new view on mechanistic aspects on antimicrobial activity, Nanomedicine: NBM 12, 789–799 (2016). doi:10.1016/j.nano.2015.11.016

44. Xu J., Tian Y., Li Z., Tan B.H., Tang K.Y., Tam K.C., β-Cyclodextrin functionalized magnetic nanoparticles for the removal of pharmaceutical residues in drinking water, J. Ind. Eng. Chem. 109, 461–474 (2022). doi:10.1016/j.jiec.2022.02.032

45. Ahmed G.H.G, Laíño R.B., Calzón J.A.G., García M.E.D., Magnetic nanoparticles grafted with β-cyclodextrin for solid-phase extraction of 5-hydroxy-3-indole acetic acid, Microchim. Acta 181, 941–948 (2014). doi:10.1007/s00604-014-1192-y

46. Banerjee S.S., Chen D.-H., Magnetic nanoparticles grafted with cyclodextrin for hydrophobic drug delivery, Chem. Mater. 19, 6345–6349 (2007). doi:10.1021/cm702278u

47. Panahi H.A., Nourbakhsh S., Siami F., Synthesis of functionalized magnetic nanoparticles as a nanocarrier for targeted drug delivery, Adv. Polym. Technol. 37, 3659–3664 (2018). doi:10.1002/adv.22150

48. Agnes M., Thanassoulas A., Stavropoulos P., Nounesis G., Miliotis G., Miriagou V., Athanasiou E., Benkovics G., Malanga M., Yannakopoulou K., Designed positively charged cyclodextrin hosts with enhanced binding of penicillins as carriers for the delivery of antibiotics: The case of oxacillin, Int. J. Pharm. 531, 480–491 (2017). doi:10.1016/j.ijpharm.2017.04.080.

49. Timofeeva L., Kleshcheva N., Antimicrobial polymers: Mechanism of action, factors of activity, and applications, Appl. Microbiol. Biotechnol. 89, 475–492 (2011). doi:10.1007/s00253-010-2920-9

50. Bansala R., Chatterjee S., Antibacterial cationic polymers: A novel approach for combating bacterial infections, Int. J. Sci. Res. Arch. 10, 611–621 (2023). doi:10.30574/ijsra.2023.10.1.0779

51. Wang L., Hu C., Shao L., The antimicrobial activity of nanoparticles: Present situation and prospects for the future, Int. J. Nanomed. 12, 1227–1249 (2017). doi:10.2147/IJN.S121956

52. Rawlinson L.B., Ryan S.M., Mantovani G., Syrett J.A., Haddleton D.M., Brayden D.J., Antibacterial effects of poly(2-(dimethylamino ethyl)methacrylate) against selected Gram-positive and Gram-negative bacteria, Biomacromolecules 11, 443–453 (2010). doi:10.1021/bm901166y

53. Gu Z., Yuan Y., He J., Zhang M., Ni P., Facile approach for DNA encapsulation in functional polyion complex for trig-gered intracellular gene delivery: Design, synthesis, and mechanism, Langmuir 25, 5199–5208 (2009). doi:10.1021/la804037v

54. Huang C-L, Lee K-M, Liu Z-X, Lai R-Y, Chen C-K, Chen W-C, Hsu J-F., Antimicrobial activity of electrospun polyvinyl alcohol nanofibers filled with poly[2-(*tert*-butylaminoethyl) methacrylate]-grafted graphene oxide nanosheets, Polymers 12, 1449 (2020). doi:10.3390/polym12071449

55. Teja A.S., Koh P.-Y., Synthesis, properties, and applications of magnetic iron oxide nanoparticles, Prog. Cryst. Growth Charact. Mater. 55, 22–45 (2009). doi:10.1016/j.pcrysgrow.2008.08.003

56. Lee H., Shin T.H., Cheon J., Weissleder R., Recent developments in magnetic diagnostic systems, Chem Rev. 115, 10690–724 (2015). doi:10.1021/cr500698d

57. Arias L.S., Pessan J.P., Vieira A.P.M., Lima T.M.T., Delbem A.C.B., Monteiro D.R., Iron oxide nanoparticles for biomedical applications: A perspective on synthesis, drugs, antimicrobial activity, and toxicity, Antibiotics 7, 46 (2018). doi:10.3390/antibiotics7020046
58. Lu Z., Yu D., Nie F., Wang Y., Chong Y., Iron nanoparticles open up new directions for promoting healing in chronic wounds in the context of bacterial infection, Pharmaceutics 15, 2327 (2023). doi:10.3390/pharmaceutics15092327
59. Ali A., Pan M., Tilly T.B., Zia M., Wu C.Y., Performance of silver, zinc, and iron nanoparticles-doped cotton filters against airborne *E. coli* to minimize bioaerosol exposure, Air Qual. Atmos. Health 11, 1233–1242 (2018). doi:10.1007/s11869-018-0622-0
60. Jagadish K., Shiralgi Y., Chandrashekar B.N., Dhananjaya B.L., Srikantaswamy S., Ecofriendly Synthesis of Metal/Metal Oxide Nanoparticles and Their Application in Food Packaging and Food Preservation, In: Impact of Nanoscience in the Food Industry, Handbook of Food Bioengineering, Eds: Grumezescu A.M., Holban A.M., Academic Press, 197–216 (2018). doi:10.1016/B978-0-12-811441-4.00008-X
61. Sahoo J., Sarkhel S., Mukherjee N., Jaiswal A., Nanomaterial-based antimicrobial coating for biomedical implants: New age solution for biofilm-associated infections, ACS Omega 7, 45962–45980 (2022). doi:10.1021/acsomega.2c06211
62. Zasońska B.A., Líšková A., Kuricová M., Tulinská J., Pop-Georgievski O., Ilavská S., Horváthová M., Jahnová E., Horák D., Functionalized porous silica&maghemite core-shell nanoparticles for applications in medicine: Design, synthesis and immunotoxicity, Croat. Med. J. 57, 165–178 (2016). doi:10.3325/cmj.2016.57.165
63. EUCAST disk diffusion method for antimicrobial susceptibility testing, version 11.0 (January 2023).
64. Patsula V., Kosinová L., Lovrić M., Ferhatovic Hamzić L., Rabyk M., Konefal R., Paruzel A., Šlouf M., Herynek V., Gajović S., Horák D., Superparamagnetic Fe_3O_4 nanoparticles: Synthesis by thermal decomposition of iron(III) glucuronate and application in magnetic resonance imaging, ACS Appl. Mater. Interfaces 8, 7238–7247 (2016). doi:10.1021/acsami.5b12720
65. Dunlop D., Özdemir Ö., Rock Magnetism: Fundamentals and Frontiers. Cambridge, UK: Cambridge University Press, Geological Magazine 135, 287–300 (1998). doi:10.1017/S0016756898218437
66. Demortiere A., Panissod P., Pichon B.P., Pourroy G., Guillon D., Donnio B., Begin-Colin S., Size-dependent properties of magnetic iron oxide nanocrystals, Nanoscale 3, 225–232 (2011). doi:10.1039/C0NR00521E

67. Babič M., Horák D., Jendelová P., Glogarová K., Herynek V., Trchová M., Likavčanová K., Hájek M., Syková E., Poly(N,N-dimethylacrylamide)-coated maghemite nanoparticles for stem cell labeling, Bioconjugate Chem. 20, 283–294 (2009). doi:10.1021/bc800373x
68. Kostiv U., Janoušková O., Šlouf M., Kotov N., Engstová H., Smolková K., Ježekb P., Horák D., Silica-modified monodisperse hexagonal lanthanide nanocrystals: Synthesis and biological properties, Nanoscale 7, 18096–104 (2015). doi:10.1039/C5NR05572E
69. Tailor S.M., Patel U.H., Synthesis, spectroscopic characterization, antimicrobial activity and crystal structure of silver and copper complexes of sulfamethazine, J. Coord. Chem. 68, 2192–2207 (2015). doi:10.1080/00958972.2015.1055258
70. Yalkowsky S.H., He Y., Jain P., Handbook of aqueous solubility data, CRC press (2016).
71. Zoppi A., Delrivo A., Aiassa V., Longhi M.R., Binding of sulfamethazine to β-cyclodextrin and methyl-β-cyclodextrin, AAPS Pharm. Sci. Tech. 14, 727–35 (2013). doi:10.1208/s12249-013-9958-9
72. Hu Q., Lu Y., Luo Y., Recent advances in dextran-based drug delivery systems: from fabrication strategies to applications, Carbohydr. Polym. 264, 117999 (2021). doi:10.1016/j.carbpol.2021.117999
73. Horwitz E.P., Gatrone R.C., Nash K.L.V., Membrane extraction with thermodynamically unstable diphosphonic acid derivatives, US Pat. 5,678,242 (1997). https://www.osti.gov/biblio/541723
74. Hajipour M.J., Fromm K.M., Ashkarran A.A, de Aberasturi D.J., de Larramendi I.R, Rojo T., Serpooshan V., Parak W.J., Mahmoudi M., Antibacterial properties of nanoparticles, Trends in Biotechnol. 30, 499–511 (2012). doi:10.1016/j.tibtech.2012.06.004
75. Zhang J., Xu Q., Li H., Zhang S., Hong A., Jiang Y., Hu N., Chen G., Fu H., Yuan M., Dai B., Chu L., Yang D., Xie Y., Self-powered electrodeposition system for sub-10-nm silver nanoparticles with high-efficiency antibacterial aktivity, J. Phys. Chem. Lett. 13, 29, 6721–6730 (2022). doi:10.1021/acs.jpclett.2c01737
76. Sondi I., Salopek-Sondi B., Silver nanoparticles as antimicrobial agent: A case study on *E. coli* as a model for Gram-negative bacteria, J. Colloid Interface Sci. 275, 177–82 (2004). doi:10.1016/j.jcis.2004.02.012
77. Yuan Y.G., Peng Q.L., Gurunathan S., Effects of silver nanoparticles on multiple drug-resistant strains of *Staphylococcus aureus* and *Pseudomonas aeruginosa* from mastitis-infected goats: An alternative approach for antimicrobial therapy, Int. J. Mol. Sci. 18, 569 (2017). doi:10.3390/ijms18030569

78. More P.R., Pandit S., Filippis A., Franci G., Mijakovic I., Galdiero M., Silver nanoparticles: Bactericidal and mechanistic approach against drug resistant pathogens, Microorganisms 11, 369 (2023). doi:10.3390/microorganisms11020369

79. Pal S., Tak Y.K., Song J.M., Does the antibacterial activity of silver nanoparticles depend on the shape of the nanoparticle? A study of the Gram-negative bacterium *Escherichia coli*, Appl Environ Microbiol. 73, 1712–20 (2007). doi:10.1128/AEM.02218-06

80. Kim J.S., Kuk E., Yu K.N., Kim J.H., Park S.J., Lee H.J., Kim S.H., Park Y.K., Park Y.H., Hwang C.Y., Kim Y.K., Lee Y.S., Jeong D.H., Cho M.H., Antimicrobial effects of silver nanoparticles, Nanomedicine 3, 95–101 (2007). doi:10.1016/j.nano.2006.12.001

81. Neal A.L., What can be inferred from bacterium-nanoparticle interactions about the potential consequences of environmental exposure to nanoparticles? Ecotoxicology17, 362–71 (2008). doi:10.1007/s10646-008-0217-x

82. Dibrov P., Dzioba J., Gosink K.K., Häse C.C., Chemiosmotic mechanism of antimicrobial activity of Ag^+ in *Vibrio cholerae*, Antimicrob. Agents Chemother. 46, 2668–2670 (2002). doi:10.1128/AAC.46.8.2668-2670.2002